

Activity and distribution of intracellular carbonic anhydrase II and their effects on the transport activity of anion exchanger AE1/SLC4A1

Samer Al-Samir¹, Symeon Papadopoulos², Renate J. Scheibe³, Joachim D. Meißner¹, Jean-Pierre Cartron⁴, William S. Sly⁵, Seth L. Alper⁶, Gerolf Gros¹ and Volker Endeward¹

¹Zentrum Physiologie, Abt. Molekular- und Zellphysiologie, AG Vegetative Physiologie 4220, Medizinische Hochschule Hannover, 30625 Hannover, Germany

²Institut für Vegetative Physiologie, Universitätsklinikum Köln, 50931 Köln, Germany

³Institut für Physiologische Chemie, Medizinische Hochschule Hannover, 30625 Hannover, Germany

⁴Institut National de la Transfusion Sanguine, 75739 Paris cedex 15, France

⁵Department of Biochemistry and Molecular Biology, St Louis University, St Louis, MO 63104, USA

⁶Renal Division, and Molecular and Vascular Medicine Division, Beth Israel Deaconess Medical Center, Harvard Medical School, 330 Brookline Avenue, Boston, MA 02215, USA

Key points

- Controversial results have been reported on the hypothesis that the cytosolic carbonic anhydrase II (CAII) of the red cell is largely bound to the cell's $\text{Cl}^-/\text{HCO}_3^-$ exchanger AE1, forming a 'metabolon complex' that greatly enhances transport activity of AE1.
- In examining so far untested aspects of this hypothesis, we report that fluorophore-labelled AE1 and CAII proteins, expressed in tsA201 cells, neither colocalize at the cell membrane nor show close proximity by Förster resonance emission spectroscopy.
- Antibody against Flag-tagged AE1 expressed in tsA201 cells co-immunoprecipitates coexpressed ankyrin but not CAII.
- CAII-deficient human red blood cells with substantial CAI activity exhibit HCO_3^- permeabilities identical to those of normal red cells.
- A mathematical model of $\text{CO}_2/\text{HCO}_3^-$ transport of red cells indicates that this process occurs more rapidly when the CA of the cell is distributed homogeneously across the cytoplasm rather than being bound to the membrane interior.

Abstract We have investigated the previously published 'metabolon hypothesis' postulating that a close association of the anion exchanger 1 (AE1) and cytosolic carbonic anhydrase II (CAII) exists that greatly increases the transport activity of AE1. We study whether there is a physical association of and direct functional interaction between CAII and AE1 in the native human red cell and in tsA201 cells coexpressing heterologous fluorescent fusion proteins CAII-CyPet and YPet-AE1. In these doubly transfected tsA201 cells, YPet-AE1 is clearly associated with the cell membrane, whereas CAII-CyPet is homogeneously distributed throughout the cell in a cytoplasmic pattern. Förster resonance energy transfer measurements fail to detect close proximity of YPet-AE1 and CAII-CyPet. The absence of an association of AE1 and CAII is supported by immunoprecipitation experiments using Flag-antibody against Flag-tagged AE1 expressed in tsA201 cells, which does not co-precipitate native CAII but co-precipitates coexpressed ankyrin. Both the CAII and the AE1 fusion proteins are fully functional in tsA201 cells as judged by CA activity and by cellular HCO_3^- permeability ($P_{\text{HCO}_3^-}$) sensitive to inhibition by 4,4'-Diisothiocyano-2,2'-stilbenedisulfonic acid.

Expression of the non-catalytic CAII mutant V143Y leads to a drastic reduction of endogenous CAII and to a corresponding reduction of total intracellular CA activity. Overexpression of an N-terminally truncated CAII lacking the proposed site of interaction with the C-terminal cytoplasmic tail of AE1 substantially increases intracellular CA activity, as does overexpression of wild-type CAII. These variously co-transfected tsA201 cells exhibit a positive correlation between cellular $P_{\text{HCO}_3^-}$ and intracellular CA activity. The relationship reflects that expected from changes in cytoplasmic CA activity improving substrate supply to or removal from AE1, without requirement for a CAII–AE1 metabolon involving physical interaction. A functional contribution of the hypothesized CAII–AE1 metabolon to erythroid AE1-mediated HCO_3^- transport was further tested in normal red cells and red cells from CAII-deficient patients that retain substantial CA activity associated with the erythroid CAI protein lacking the proposed AE1-binding sequence. Erythroid $P_{\text{HCO}_3^-}$ was indistinguishable in these two cell types, providing no support for the proposed functional importance of the physical interaction of CAII and AE1. A theoretical model predicts that homogeneous cytoplasmic distribution of CAII is more favourable for cellular transport of HCO_3^- and CO_2 than is association of CAII with the cytoplasmic surface of the plasma membrane. This is due to the fact that the relatively slow intracellular transport of H^+ makes it most efficient to place the CA in the vicinity of the haemoglobin molecules, which are homogeneously distributed over the cytoplasm.

(Received 7 January 2013; accepted after revision 17 July 2013; first published online 22 July 2013)

Corresponding authors G. Gros: Zentrum Physiologie, Vegetative Physiologie 4220, Medizinische Hochschule Hannover, Carl-Neuberg-Str. 1, 30625 Hannover, Germany. Email: Gros.Gerolf@MH-Hannover.de; V. Endeward: Zentrum Physiologie 4220, Medizinische Hochschule Hannover, Germany. Email: Endeward.Volker@MH-Hannover.de.

Abbreviations A_{CA} , carbonic anhydrase activity; AE1, SLC4A1, anion exchanger 1; A_i , intracellular carbonic anhydrase activity; ANK1, ankyrin 1; CA, carbonic anhydrase; CAII, carbonic anhydrase isoform II; Co-IP, co-immunoprecipitation; FRET, Förster resonance energy transfer; $P_{\text{HCO}_3^-}$, membrane HCO_3^- permeability; P_{CO_2} , membrane CO_2 permeability; tsA201, SV40-transformed HEK293 cells.

Introduction

The erythroid $\text{Cl}^-/\text{HCO}_3^-$ exchanger 1 (AE1/SLC4A1) is responsible for the so-called Hamburger shift, which exchanges Cl^- for HCO_3^- across the red cell membrane during the blood's CO_2 uptake in the tissue and CO_2 release in the lung. This mechanism results in a major augmentation of the CO_2 binding capacity of the blood by mediating transfer into the plasma of a major part of the HCO_3^- that is formed from CO_2 inside red blood cells (RBCs) by the action of intracellular carbonic anhydrase (CA).

The present study addresses the question of whether carbonic anhydrase II (CAII) in the human red cell is largely bound to the internal side of the plasma membrane, specifically to the short cytoplasmic C-terminal tail of AE1 (see Fig. S1, Supplemental Data). The study additionally examines the hypothesis, originally proposed by Vince and Reithmeier (1998), that CAII binding to AE1 activates the latter such that the two proteins form a 'metabolon' mediating enhanced HCO_3^- transport across the red cell membrane.

It was postulated long ago that substantial CAII is bound to the interior of the red cell membrane (Enns, 1967). Subsequent investigations with red cell ghosts repeatedly washed before resealing led three groups to conclude that

various wash procedures removed CAII almost completely from the red cell membrane (Rosenberg & Guidotti, 1968; Tappan, 1968; Randall & Maren, 1972). These latter studies together suggested the absence of a high affinity association between CAII and the cytoplasmic surface of the red cell membrane.

However, Parkes and Coleman (1989) later observed that addition of human red cell ghost fragments increased human CAII activity by 3.5-fold. Kifer *et al.* (1993) reported that addition of DIDS (4,4'-Diisothiocyano-2,2'-stilbenedisulfonic acid; presumed to bind mainly to AE1) altered the fluorescence of dansylsulfonamide bound to intra-erythrocyte CA, consistent with direct interaction between AE1 and CAII. Vince and Reithmeier (1998) then revived interest in the field with the following findings:

- (1) in (unwashed) red cell ghosts CAII immunofluorescence was predominantly detected close to the membrane inner surface (as also reported in confocal images of intact erythrocytes by Campanella *et al.* 2005). Tomato lectin application to red cell ghosts caused clustering of both AE1 and CAII, although colocalization of AE1 and CAII in these clusters was not demonstrated;

- (2) CAII and AE1 could be co-immunoprecipitated with antibody recognizing the N terminus of AE1 (but not with antibody recognizing the AE1 C terminus);
- (3) a solid phase binding assay revealed binding of detergent-solubilized intact band 3 to immobilized CAII with K_d of 70 nM, and binding was inhibited by antibody against the AE1 C terminus;
- (4) another solid-phase binding assay showed an interaction of immobilized CAII with soluble phase AE1 C-terminal cytoplasmic tail (Ct) fused at its N-terminal end with glutathione-S-transferase (GST). This enzyme-linked immunosorbent assay (ELISA) later identified the CAII binding region within the AE1-Ct as the four residues 887DADD890 (Vince & Reithmeier, 2000). The authors pointed out that AE1 transporters of many other species show the same or very similar sequences, e.g. DGDD in mouse and rat and DADD in bovine RBCs (Fig. S1). The elements essential for binding were three, or at least two, negatively charged Asp residues within these four amino acids, always preceded by an aliphatic residue. The GST-AE1-Ct ELISA also revealed within the N-terminal 17 residues of CAII a binding site of six positively charged His or Lys residues, proposed to interact with the AE1 C-terminal cytoplasmic tail DADD motif described above (Vince *et al.* 2000; see Fig. S1). CAI, which lacks all of these six residues, did not bind to AE1. A corollary of these studies derives from (i) the presence in human red cells of $\sim 10^6$ copies of AE1 and $\sim 10^6$ copies of CAII (yielding an $\sim 20 \mu\text{M}$ CAII concentration if distributed throughout the cytosolic volume), and from (ii) the above mentioned 70 nM K_d for binding of AE1 and CAII. These values predict an intra-erythrocyte equilibrium concentration of unbound (free cytosolic) CAII of only $1.2 \mu\text{M}$, implying that 94% of RBC CAII should be AE1-bound, and thus effectively membrane-bound. In contrast, Piermarini *et al.* (2007) in a reinvestigation reported no detectable *in vitro* binding interaction between a synthetic AE1-C-terminal peptide and CAII as assayed either by ELISA or by surface plasmon resonance.

While the results of Reithmeier and colleagues strongly suggest significant binding of CAII to AE1, formation by the two interacting proteins of a 'metabolon' (i.e. with enhancement of the transport function of AE1) remained an open question. Such enhancement could occur through an allosteric effect of CAII binding on AE1, potentially independent of CAII enzymatic activity, or through the close proximity of CA catalytic activity to the intracellular substrate transport site of AE1, effectively allowing instantaneous conversion of HCO_3^- to CO_2 after anion translocation, and thus maintaining an optimal transmembrane HCO_3^- gradient. The latter mechanism could

require either simple proximity of the AE1 transport site and CAII catalytic activity, or it could imply a more specific interaction between the AE1 transport site and the catalytic centre of CAII to facilitate HCO_3^- translocation across the permeability barrier within the AE1 polypeptide.

A first test of functional interaction between CAII and AE1 activity was reported by Sterling *et al.* (2001a,b), who overexpressed AE1 in HEK293 cells containing endogenous CAII. They found that: (i) the CA inhibitor acetazolamide reduced the stimulation of $\text{Cl}^-/\text{HCO}_3^-$ exchange by extracellular Cl^- removal and restoration, respectively, by 50%, thus showing that CAII activity accelerates AE1 activity; (ii) AE1 with mutated DADD (the proposed CAII binding site in the C-terminal cytoplasmic tail) exhibited 90% reduction of transport activity in HEK293 cells, which they attributed to reduced AE1 binding of CAII (however, transport activities of these mutants were not tested in the absence of CAII); and (iii) in HEK293 cells cotransfected with cDNA encoding the catalytically inactive CAII-V143Y mutant resulted in a 60% reduction of AE1 transport rates, interpreted as reflecting displacement of endogenous CAII of HEK293 cells from its AE1 binding site by the inactive heterologous mutant CAII. The implication of this interpretation is that CAII binding to AE1 is required to enhance AE1 transport activity.

The present study reinvestigates the AE1–CAII metabolon hypothesis by probing the following questions that have not been examined to date:

1. Is fluorophore-labelled CAII in intact cells expressing heterologous AE1 indeed concentrated predominantly at the internal side of the plasma membrane, as postulated for RBCs? We investigate this by expressing yellow fluorescent protein-labelled AE1 in tsA201 cells (SV40-transformed HEK293 cells) and studying the distribution of coexpressed cyan fluorescent protein-labelled CAII using confocal microscopy.
2. Is CAII directly bound to AE1? We probe this by studying Förster resonance energy transfer (FRET) between the two coexpressed fusion proteins.
3. Can association between native CAII and AE1 be demonstrated by co-immunoprecipitation of the two proteins when expressed in tsA201 cells?
4. What is the effect of coexpressing the catalytically inactive CAII mutant V143Y on HCO_3^- transport by intact AE1-expressing tsA201 cells? How can the results be interpreted, when total intracellular CA activity is taken into account?
5. What is the effect of expressing a truncated CAII whose N-terminal amino acids 1–24 have been deleted (Fig. S1), thereby removing all proposed AE1 binding residues of CAII and thus preventing the proposed AE1 binding to the CAII N terminus?

6. Is concentration of CA activity at the inner face of the plasma membrane indeed better for maximizing $\text{Cl}^-/\text{HCO}_3^-$ exchange activity than a homogeneous cytoplasmic distribution of CA activity? We address this problem by applying a mathematical model simulating membrane transport in conjunction with intracellular diffusion and reaction processes of CO_2 , HCO_3^- and H^+ .
7. Does AE1-mediated HCO_3^- transport in CAII-deficient human red cells differ from that in normal human red cells? This is an interesting model in which to test the metabolon hypothesis, because CAII-deficient RBCs still express substantial CA activity due to CAI which, however, does not bind to AE1.

Methods

Blood samples

Human red cells were taken from several members of our laboratory and used for mass spectrometric experiments on the same and the following day. Repeating the measurement 4 days after taking the blood made no difference in terms of mass spectrometric records. Two different CAII-deficient blood samples were taken from a member of a US family (CAII deficiency due to a 145–148 GTTT del mutation in exon 2; Shah *et al.* 2004) and from an Arabian patient (CAII deficiency due to a point mutation (G→A transition) at the exon 2–intron 2 junction; Hu *et al.* 1992). All red cells were washed three times in physiological saline before being used in the mass spectrometric experiments and were controlled for haemolysis. Haematocrit and blood cell count were taken to determine mean corpuscular volumes. Informed consent was sought and given in accordance with the Declaration of Helsinki. CAII-deficient blood samples were shipped chilled and red cells were used within 2–4 days after the samples were taken.

Cell culture

The tsA201 cell line was obtained from the European Collection of Cell Cultures. The cells were cultured in DMEM supplemented with 2 mM L-glutamine, 10% fetal bovine serum and penicillin/streptomycin at 37°C in 5% CO_2 . For confocal laser scanning microscopy the cells were seeded on 35 mm (9.6 cm²) glass bottom dishes (MatTek Corp., Ashland, MA 01721, USA) with 2 ml culture medium and $\sim 8 \times 10^4$ cells per ml culture medium. For mass spectrometric measurements the cells were seeded on 100 mm (78.5 cm²) plastic dishes with 10 ml culture medium and $\sim 4.3 \times 10^4$ cells per ml culture medium. For Western blot analysis, cells were seeded in an 80 cm² cell culture flask with 20 ml culture medium and 4.3×10^4 cells per ml medium.

Transfection with fusion proteins

Cells were transfected according to the manufacturer's protocol with GeneJuice (Novagen, Merck, Darmstadt, Germany). YPet-mAE1, YPet-hAE1, CAII-CyPet, CAII-V143Y-CyPet or truncated CAII-CyPet (truncation of the N terminus of CAII, see Fig. S1) were transfected or co-transfected in different combinations of mAE1 and CAII. For transfections, 6 µg of each plasmid was applied per dish. For confocal laser scanning microscopy, transfection was done 24 h after seeding, and for mass spectrometric measurements 48 h after seeding. Transfection efficiency was 30–40%.

Construction of CyPet- and YPet-tagged AE1 and CAII

The yellow and cyan fluorescent tags used in this study are fluorescent protein variants optimized for FRET and encoded by the vectors pECyPet-N1 and pEYPet-C1, kindly provided by Dr Patrick S. Daugherty, University of California, Santa Barbara (Nguyen & Daugherty, 2005). For AE1 tagged N-terminally with YPet, an *XhoI-SalI* PCR product of the human AE1 and *XhoI-EcoRI* PCR product of murine AE1 were generated using Taq DNA Polymerase (New England Biolabs, Ipswich, MA, USA). The recognition sequences of the restriction endonucleases were added up- and downstream of the AE1 cDNA sequence using PCR primers. The resulting products were gel-purified and ligated 3' into the pEYPet-C1 vector cut with suitable endonucleases.

For C-terminal tagging of the CAII constructs with CyPet, a *BglII-SalI* PCR product of human CAII was generated as described above. The stop codon was replaced with the amino acid tryptophan. The PCR product was ligated into vector pECyPet-N1.

The truncated CAII was produced by PCR-mediated deletion of codons 1–24, encoding the reported binding site for the AE1 C-terminal sequence DADD (Vince *et al.* 2000). The PCR product was ligated into the host vector as described above.

The CAII-V143Y cDNA (encoding a mutant polypeptide with enzymatic activity 3000-fold lower than that of wild-type CAII; Fierke *et al.* 1991) kindly provided by Dr Joe Casey, University of Alberta, was ligated into pECyPet-N1 as described above. To obtain an AE1 construct labelled at both the N and the C terminus, the *XhoI-EcoRI* PCR product encoding the murine AE1 with the stop codon replaced by glycine was subcloned into a CyPet-YPet tandem protein expression vector, upon opening of the latter between the CyPet and YPet sequence via an *XhoI/EcoRI* double digest. This procedure produced CyPet-AE1-YPet, which we used as a membrane-associated, positive FRET control.

Confocal microscopy and FRET measurements

Twenty-four (or occasionally 48) hours post-transfection, the culture dishes were mounted onto the stage of an inverse FV1000 confocal laser-scanning microscope (Olympus Deutschland, Hamburg, Germany), and cells were observed under oil immersion using a 60 \times objective. CyPet and YPet were excited using a 440 nm blue diode and the 514 nm argon line, respectively, directed to the cells via a 458/514 nm dual dichroic mirror. CyPet and YPet emission intensities were photometrically detected using Olympus filters BA465-495 and BA535-565, respectively. When simultaneous excitation of both CyPet and YPet was desired (as in Fig. 5A, see below) the excitation wavelength was 458 nm.

The experimental procedure to check for FRET was as described by Papadopoulos *et al.* (2004), who demonstrated the close proximity of regions of two proteins from determinations of FRET with dyes similar to those applied here. In brief, the intensity of CAII-CyPet emission (I_{Cy}) during excitation with the 440 nm line was measured photometrically before ($I_{Cy,Pre}$) and after ($I_{Cy,Post}$) complete bleaching of the potential FRET acceptor YPet-mAE1. Bleaching was conducted using the full laser power (100% setting) of the 514 nm argon line, a wavelength close to the excitation maximum of YPet, but with no excitation of CyPet. The entire cell was subjected to bleaching, but $I_{Cy,Post}$ and $I_{Cy,Pre}$ were determined exclusively for regions populated with the potential energy acceptor YPet-mAE1, i.e. at the cell membrane. In analysing an acceptor bleaching experiment, the finding of $I_{Cy,Post} > I_{Cy,Pre}$ would indicate pre-bleach energy transfer from CAII-CyPet to YPet-mAE1. Since the latter phenomenon is measurable only when the two fluorophores are separated by <8–10 nm, FRET in this case would confirm the close proximity of CAII and mAE1, compatible with direct, physical interaction.

Co-immunoprecipitation (Co-IP)

An expression vector for 3xFlag-tag attached to the N terminus of the human anion exchanger 1 (hAE1) was generated by cloning 3xFlag-tagged hAE1 cDNA, generated by PCR using forward (F), 5'-CTGTCAAAGCTTATGGACTACAAAGACCATGACGGTGATTATAAA GATCATGACATCGATTACAAGGATGACGATGACAAGCTAGTGGAGGAGCTGCAGGATGA-3', and reverse (R), 5'-CTGTCACTCGAGTCACACAGGCATGGCCACTT-3', primers, into pcDNA3 (Invitrogen, Karlsruhe, Germany). A human ankyrin 1 (hANK1) expression vector was generated by cloning hANK1 cDNA (a gift from Dr V. Bennett), generated by PCR using F, 5'-ACGTGGTACCATGCCCTATTCTGTGGGCTTCC-3', and R, 5'-ACTGGAATTCTTAAACCTTATCGTCGTCATCC-3', primers into pcDNA3.

tsA201 cells were transfected at 70–80% confluence in serum-free DMEM with 6 μ g pcDNA3–3xFlag-hAE1 expression plasmid and 6 μ g pcDNA-hANK1 expression plasmid or empty expression vector, and 3 μ l μ g⁻¹ DNA of Gene Juice transfection reagent (Novagen) in 100 mm dishes. After 24 h, the transfection medium was changed to DMEM. After a further 24 h, cells were harvested and washed once with ice-cold PBS. After addition of 500 μ l IP-lysis buffer (50 mM Tris-HCl, pH 7.5, 1 mM EGTA, pH 7.0, 1 mM EDTA, 10 mM glycerol phosphate, 50 mM sodium fluoride, 1 mM sodium orthovanadate, 5 mM sodium pyrophosphate, 1% Triton X-100, 0.27 M saccharose, 1 tablet cOmplete Mini, EDTA-free Protease Inhibitor Cocktail (Roche Applied Science, Mannheim, Germany)/10 mL buffer), cells were scraped, vortexed, and after 20 min on ice, centrifuged for 20 min (13,000 r.c.f.) at 4°C. The supernatant (lysate) was stored at –80°C.

Anti-Flag M2 affinity gel suspension (30 μ l; Sigma-Aldrich, Taufkirchen, Germany) was washed three times with 1 ml IP-buffer (centrifugation for 5 min at 3500 r.c.f., 4°C). The affinity gel was resuspended with 200 μ l IP-lysis buffer and 500 μ l cell lysate was added. After incubation overnight at 4°C in an overhead shaker, the affinity gel was centrifuged and washed five times with 1 ml IP-buffer. The supernatant of the first centrifugation was stored at –80°C for Western blot analysis.

For Western blot analysis, the affinity gel was incubated for 20 min at 37°C with 20 μ l 2 \times SDS sample buffer, cooled on ice and centrifuged at 4°C. The supernatant (eluate) was run on a 10% SDS-PAGE and analysed using anti-ANK1 (Santa Cruz Biotechnology, Inc., Heidelberg, Germany), anti-CAII (Acris Antibodies, Herford, Germany) and anti-Flag (Stratagene, Agilent Technologies, Waldbronn, Germany) antibodies (CAII ~ 29 kDa; hANK1 ~ 200 kDa; 3xFlag-hAE1 ~ 98 kDa).

Mass spectrometric determination of bicarbonate permeability and cellular CA activity

This method was described in detail previously (Endeward & Gros, 2005; Endeward *et al.* 2006). Suspensions of human red cells (final haematocrit 0.03%) or tsA201 cell (final cytocrit 0.3%) were used in the mass spectrometric chamber at constant pH of 7.40 and temperature of 37°C. Briefly, in the presence of a solution of ¹⁸O-labelled HCO₃⁻ the time course of the decay of C¹⁸O¹⁶O in the suspension was followed via the special mass spectrometric inlet system described earlier. From these time courses (e.g. as shown in Endeward *et al.* 2008; Endeward & Gros, 2009), the permeabilities of the cells for HCO₃⁻, $P_{HCO_3^-}$, and CO₂, P_{CO_2} , were obtained in two steps: (1) preliminary estimates of $P_{HCO_3^-}$ and P_{CO_2} were inserted into the set of differential equations describing the process of ¹⁸O exchange (as given by Endeward & Gros, 2005) and used to calculate a 'theoretical' curve of C¹⁸O¹⁶O

decay; (2) this calculated curve was compared with the experimental decay curve, and parameters $P_{\text{HCO}_3^-}$ and P_{CO_2} were varied by a fitting procedure, again as described by Endeward and Gros (2005), until the pair of $P_{\text{HCO}_3^-}$ and P_{CO_2} values was obtained that best described the experimental curve. Usually, the fit produces a curve of $\text{C}^{18}\text{O}^{16}\text{O}$ decay that is virtually indistinguishable from the experimental curve (Endeward & Gros, 2009). The sensitivity of the fitted values of $P_{\text{HCO}_3^-}$ to the parameters used in the differential equations has been described previously (Endeward *et al.* 2008). Figure 1A shows that, for a given P_{CO_2} , the minimum of the sum of squared deviations between the $\text{C}^{18}\text{O}^{16}\text{O}$ concentrations of the experimental decay curves and those of the curves calculated from

the fit defines $P_{\text{HCO}_3^-}$ very well. Figure 1B shows that the experimental data allow us equally well to derive the optimal combination of $P_{\text{HCO}_3^-}$ and P_{CO_2} values. In Fig. 1A and B there is one single minimum for the sum of squares and no local minima whatsoever.

Evaluation of $P_{\text{HCO}_3^-}$ from the time courses of $\text{C}^{18}\text{O}^{16}\text{O}$ requires knowledge of the intracellular CA activity (Endeward & Gros, 2005). This was obtained by lysing cell suspensions of defined haematocrit or cytocris, followed by centrifugation at 100,000 *g* (1 h), and determining the CA activity of the solutions by mass spectrometry. Conditions were 37°C and, approximating intracellular conditions, pH 7.20 with final Cl^- concentrations of 60 mM for haemolysates and 10 mM for tsA cell lysates.

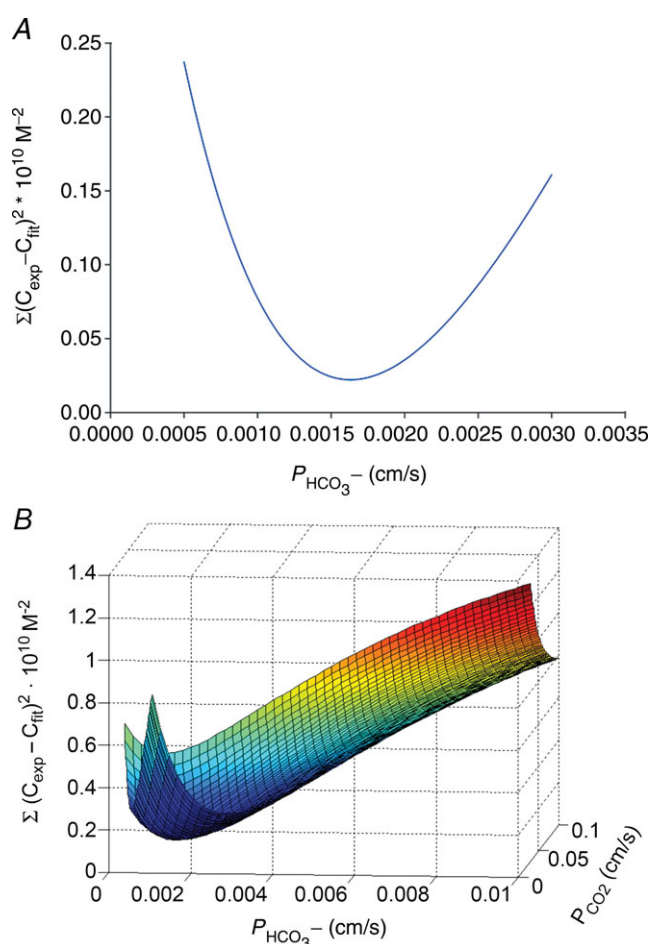


Figure 1. Determination of $P_{\text{HCO}_3^-}$ and P_{CO_2} from the mass spectrometric records by minimizing the sum of squared deviations

$P_{\text{HCO}_3^-}$ – Illustration of the fitting procedure used to determine $P_{\text{HCO}_3^-}$ at a given P_{CO_2} of 0.12 cm s^{-1} (A) or both P_{CO_2} and $P_{\text{HCO}_3^-}$ (B). The sum of squares of deviations between experimental concentrations of $\text{C}^{18}\text{O}^{16}\text{O}$ and their counterparts from the calculated $\text{C}^{18}\text{O}^{16}\text{O}$ decay curve as obtained with the fitted values of $P_{\text{CO}_2}/P_{\text{HCO}_3^-}$ are plotted vs. the value of $P_{\text{HCO}_3^-}$ (A) or vs. both the values of $P_{\text{HCO}_3^-}$ and P_{CO_2} (B).

Statistical analysis

Statistical significance was tested by Student's *t* test where applicable, or by ANOVA followed by a suitable post-test (Bonferoni, comparing selected pairs of data groups, or Tukey, for multiple comparisons).

Mathematical Model of HCO_3^- and CO_2 transport across cell membranes

The purpose of this mathematical model is to simulate the processes of CO_2 and HCO_3^- transfer across the cell membrane, together with the associated diffusion and reaction processes in the intracellular space (see Fig. S2). The transfer of CO_2 or HCO_3^- across the membrane is given by:

$$dm_{X,M}/dt = -P_X \cdot A \cdot d[X], \quad (1)$$

where $dm_{X,M}$ is the amount of X (either CO_2 or HCO_3^-) transferred across the membrane per unit time, P_X is the membrane permeability of CO_2 or HCO_3^- , respectively, A is the membrane diffusion area (140 μm^2 for a human red cell; Geigy, 1960) and $d[X]$ is the concentration difference across the membrane for either of the two substrates. The rates of the CO_2 hydration–dehydration reaction in the intracellular compartment are described by:

$$d[\text{CO}_2]/dt = -k_u \cdot A_{\text{CA}} \cdot [\text{CO}_2] + (k_u \cdot A_{\text{CA}}/K_1') \cdot [\text{H}^+] \cdot [\text{HCO}_3^-], \quad (2)$$

where k_u is the forward reaction rate constant of CO_2 hydration (0.15 s^{-1} at 37°C; cf. Endeward & Gros, 2009), A_{CA} is the factor by which this reaction rate is accelerated due to CA, $[\text{CO}_2]$, $[\text{H}^+]$ and $[\text{HCO}_3^-]$ are the concentrations of physically dissolved CO_2 , of protons and HCO_3^- , respectively, t is time, and K_1' is the first apparent dissociation constant of carbonic acid (7.9×10^{-7} M at 37°C). K_1' treats the CO_2 hydration reaction by assuming a direct conversion of CO_2 and H_2O to HCO_3^- and H^+ (omitting the intermediate H_2CO_3),

which is correct in the case of the CA-catalysed reaction but constitutes a (generally employed) simplified description of the uncatalysed reaction. As indicated in Fig. S2 (upper part), in the standard case CA was assumed to be homogeneously distributed in the intracellular space; in special cases all intracellular CA was assumed to be concentrated in the immediate neighbourhood of the internal side of the membrane (Fig. S2, lower part). An equation analogous to eqn (2) is used to describe the change of HCO_3^- concentration per time, $d[\text{HCO}_3^-]/dt$. The intracellular diffusion processes of CO_2 and HCO_3^- are expressed by:

$$dm_X/dt = -D_X \cdot A \cdot d[X]/dx, \quad (3)$$

where dm_X/dt indicates the movement of substance per unit time between small volume elements of the intracellular space, D_X is the diffusion coefficient in the intracellular space, A is the diffusion area between the volume elements considered, and $d[X]/dx$ is the concentration gradient of CO_2 or HCO_3^- , respectively. D_{CO_2} was taken be $1.2 \times 10^{-5} \text{ cm}^2 \text{ s}^{-1}$, and $D_{\text{HCO}_3^-}$ $0.6 \times 10^{-5} \text{ cm}^2 \text{ s}^{-1}$ (cf. Endeward & Gros, 2009). A modified version of eqn (3) had to be used to describe intracellular diffusion of H^+ , which, due to the extremely low intracellular concentrations and concentration gradients of free H^+ , occurs almost entirely by haemoglobin-facilitated proton diffusion (Gros & Moll, 1972, 1974; Gros *et al.* 1976):

$$dm_{\text{H}^+}/dt = -D_{\text{Hb}} \cdot \text{BF} \cdot A \cdot dpH/dx, \quad (4)$$

where dm_{H^+}/dt is the total amount of protons transferred across the segment at the considered position x , D_{Hb} is the intra-erythrocytic diffusion coefficient of haemoglobin ($6.4 \times 10^{-8} \text{ cm}^2 \text{ s}^{-1}$ at 37°C ; Moll, 1966), BF is the intra-erythrocytic non-bicarbonate buffering power in moles $\text{H}^+/\text{L}/\Delta\text{pH}$, mainly due to haemoglobin ($63 \text{ mm}/\Delta\text{pH}$), and dpH/dx is the intracellular pH gradient. The minor contribution of the intra-erythrocytic buffers of lower molecular weight (2,3-bisphosphoglycerate, 2,3-BPG, and adenosine triphosphate, ATP) is ignored in this treatment.

This system of equations is largely analogous to that used previously to describe the exchange of $\text{C}^{18}\text{O}^{16}\text{O}$ between red cells and the extracellular space (Endeward & Gros, 2009), with the exception of proton transport, which did not have to be considered in the earlier model. Also, unlike the treatment there, the extracellular space was treated here as a well-stirred compartment of infinite size, and unstirred layers around the cells were not considered. The example of a cell considered here was the human RBC, whose parameters were inserted into the equations (for details see Endeward & Gros, 2009). The diffusion and reaction processes in the intracellular compartment were modelled by dividing the effective half-thickness of the erythrocyte of $0.8 \mu\text{m}$ (Forster, 1964) into 80 segments, as indicated in Fig. S2, and with these a finite difference

method (as available in MATLAB 2008b) was used to solve the equations numerically.

The equations were solved in such a way as to obtain the amount of substance, i.e. CO_2 or HCO_3^- , taken up into the cell per unit membrane area (in units of moles cm^{-2}) as a function of time (as shown in Figs 8 and 9). The fact that HCO_3^- transfer across the cell membrane approaches an intracellular HCO_3^- concentration that is not equal to but in Donnan equilibrium with the extracellular concentration was taken into account as described previously (Itada & Forster, 1977; Endeward & Gros, 2005). The condition of maintaining the Donnan distribution for HCO_3^- has also the consequence that HCO_3^- uptake is accompanied by a CO_2 efflux (as seen in Fig. 9B).

Results

Co-IP of AE1 and CAII

To investigate a possible direct physical interaction between AE1 and CAII in tsA201 cells, a Co-IP assay was performed using an anti-Flag affinity gel. In lysates from tsA201 cells transiently expressing Flag-tagged hAE1, nearly no Co-IP of CAII was found (Fig. 2, right-hand column). Instead, the bulk of CAII protein remained in the supernatant of the Co-IP assay. As a positive control for Co-IP, a protein well known for interaction with hAE1, hANK1 (Bennett & Stenbuck, 1979; Michaely & Bennett, 1995), was coexpressed with Flag-tagged hAE1. Figure 2 shows that hANK1 was indeed co-immunoprecipitated with hAE1, constituting a positive control of the assay. Therefore, the Co-IP assay demonstrates that AE1 and CAII do not interact in tsA cells.

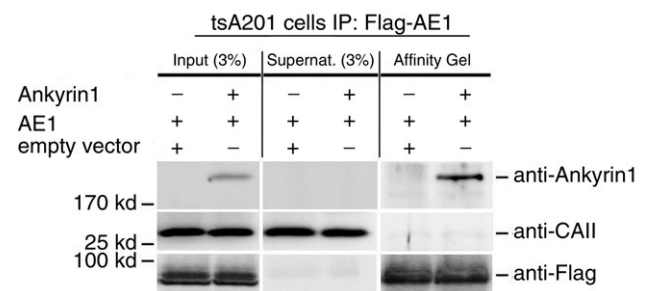


Figure 2. Co-immunoprecipitation (Co-IP) demonstrates interaction of AE1 with ANK1, but not with CAII

Western blot analysis of aliquots from cell lysates (Input; 3% of the volume of cell lysate added to the affinity gel was applied to the SDS-PAGE gel) from tsA201 cells transfected with pcDNA3-3xFlag-hAE1 expression plasmid (AE1) and pcDNA-hANK1 expression plasmid (Ankyrin) or empty expression vector (empty vector), of aliquots from supernatants of the Co-IP (Supernat.; 3% of the supernatant after centrifugation of the affinity gel was applied to the SDS-PAGE gel), and of eluates from the affinity gel (all of the eluate was applied to the SDS-PAGE gel), using anti-ANK1, anti-CAII or anti-Flag antibodies.

Expression, localization and FRET signal of YPet-AE1 and CAII-CyPet coexpressed in tsA cells

Western Blots were performed as described by Itel *et al.* (2012) and illustrate in the supplementary Fig. S3 the expression of native CAII and of the fusion proteins CAII-CyPET (see also Fig. 3A) and CAII-V143Y-YPet (see also supplemental Fig. S4b) in tsA201 cells. The molecular mass of the two latter proteins was the expected ~ 57 kDa. Figure 3A shows the subcellular localizations of CAII-CyPet (left) and murine YPet-mAE1 (right). It is apparent that the AE1 fusion protein is enriched at the plasma membrane of the tsA cell, with some minor association with intracellular vesicular structures, whereas the CAII fusion protein is homogeneously distributed throughout the cytoplasm, without evident enrichment at the plasma membrane. This is confirmed by the fluorescence intensity profiles of Fig. 3B that were recorded along the red lines shown in Fig. 3A. YPet-mAE1 exhibits low fluorescence intensity in the cytoplasm and marked intensity peaks associated with the plasma membranes. CAII-CyPet shows a high and rather homogeneous intensity across the cell cytoplasm region without enrichment of fluorescence intensity in the region of the plasmalemma. The same distribution pattern is seen for CAII-CyPet and human YPet-hAE1 in Fig. 3C. This suggests that the CAII fusion protein behaves as a typical cytosolic protein without detectable enrichment at the plasma membrane. Figure 3D shows that in a patch of doubly transfected confluent tsA201 cells, regions containing non-transfected cells free of either blue or yellow fluorescence can serve as negative fluorescence controls.

So as not to overlook subtle interactions between CAII and AE1, we checked for evidence of FRET. As described in the Methods, the potential FRET acceptors YPet-mAE1 and YPet-hAE1 were bleached, after which the cells were examined for possible increase in FRET donor emission ($I_{\text{Cy,post}}$) over their pre-bleaching value $I_{\text{Cy,pre}}$. An increase in $I_{\text{Cy,post}}$, expressed in Fig. 4B as FRET ratio $= (I_{\text{Cy,post}} - I_{\text{Cy,pre}}) / I_{\text{Cy,post}}$, was never observed in cells coexpressing CAII-CyPet with either YPet-mAE1 or YPet-hAE1 (Fig. 4B). The absence of FRET is evidence against physical interaction of CAII fusion protein with AE1 fusion protein. In contrast, in tsA201 cells expressing the intramolecular FRET control construct CyPet-mAE1-Ypet, YPet bleaching elicited a significant increase in CyPet fluorescence intensity (Fig. 4B). The double-tagged mAE1 thus constitutes a positive FRET control, validating the negative results with the single-tagged CAII and AE1 fusion proteins. The double-labelled mAE1 construct is illustrated in Fig. 4A, in which excitation at 458 nm produced simultaneous blue and yellow fluorescence emission of the membrane-associated mAE1.

Figure S4 demonstrates that both CAII constructs, that truncated at the N terminus and the acatalytic CAII-V143Y, are well expressed, exhibit a cytosolic distribution identical to that of the WT CAII fusion protein shown in Fig. 3, and do not affect expression of AE1. Thus, all tested WT and mutant CAII fusion proteins expressed here are homogeneously distributed in the cytoplasm and exhibit no enrichment at the plasma membrane.

Functional effects of the expression of YPet-mAE1 in tsA201 cells

Figure 5 shows that the AE1 fusion protein is functional in tsA201 cells. Figure 5A shows that the CA activity (acceleration factor of CO_2 hydration minus 1) of lysed tsA201 cells as measured by ^{18}O mass spectrometry is slightly over 600 in control as well as in AE1-expressing tsA cells (37°C). Figure 5B presents ^{18}O mass spectrometric determinations of $P_{\text{HCO}_3^-}$ in tsA201 cells. Control cells exhibit a $P_{\text{HCO}_3^-}$ of $\sim 2 \times 10^{-4} \text{ cm s}^{-1}$ (37°C), and this value is not significantly altered in the presence of 10^{-5} M DIDS, indicating that AE1 is not responsible for the basal HCO_3^- permeability of tsA cells. Expression of the AE1 fusion protein almost doubles $P_{\text{HCO}_3^-}$ ($P < 0.02$), and DIDS restores this value to control level ($P < 0.02$). We conclude that the AE1 fusion protein is functional when expressed in tsA cells, markedly increasing cellular HCO_3^- permeability.

Bicarbonate permeabilities of tsA201 cells expressing YPet-mAE1 together with various CAII-CyPet fusion proteins

Figure 6 shows $P_{\text{HCO}_3^-}$ values measured in AE1-transfected tsA201 cells coexpressing fluorophore-labelled WT-CAII, truncated CAII and the acatalytic CAII mutant, and plotted *vs.* corresponding lysate CA activities measured as described above. All data points shown in Fig. 6 are mean values from several preparations. First, the figure shows that expression of tagged WT-CAII as well as of tagged truncated CAII results in enhanced cytosolic CA activity, but expression of CAII-V143Y does not. Secondly, the data are well described by a linear regression line consistent with a positive correlation of $P_{\text{HCO}_3^-}$ and intracellular CA activity. The second point from the left (\blacktriangledown) represents tsA201 cells expressing mAE1 together with endogenous CAII only (the conditions of Fig. 5A, right column, and Fig. 5B, third column, which we will call here 'control' conditions) with $P_{\text{HCO}_3^-}$ of $4.3 \times 10^{-4} \text{ cm s}^{-1}$. The leftmost data point (\blacktriangle) representing expression of acatalytic CAII (see Fig. S4b) with $P_{\text{HCO}_3^-}$ of $3.4 \times 10^{-4} \text{ cm s}^{-1}$ is moderately but significantly lower than the control value ($P < 0.02$), and unexpectedly shows marked reduction in endogenous intracellular CA activity. We have confirmed this effect of expression of the

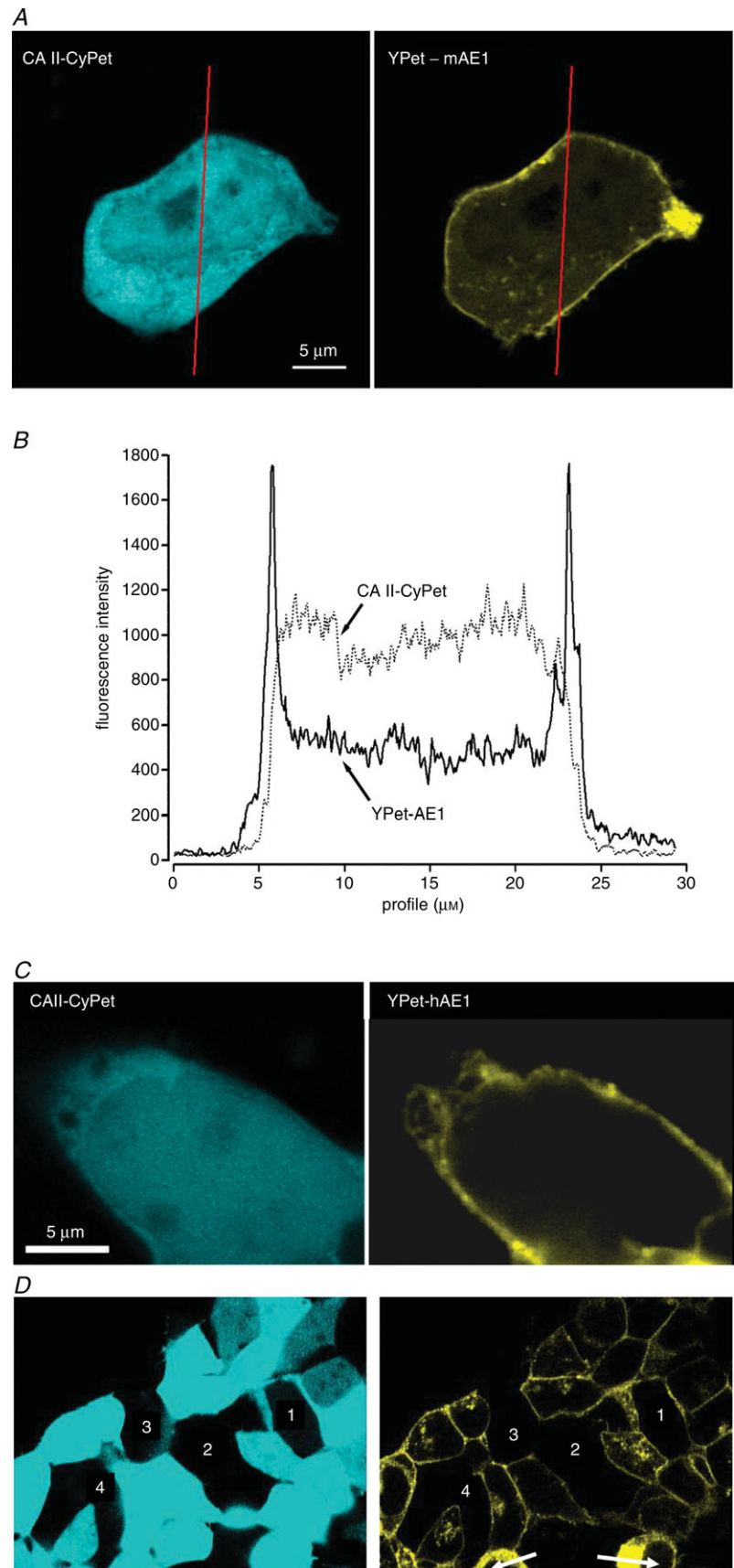


Figure 3. Confocal microscopy of the fluorescent fusion proteins CA II and AE1

A, confocal microscopic images of a tsA291 cell co-transfected with human CAII-CyPet and murine YPet-AE1 fusion proteins. CyPet was linked to the C terminus of CAII and YPet was linked to the N-terminus of mAE1 **B**, fluorescence emission intensity profiles at wavelengths appropriate for CyPet and for YPet as recorded along the red lines in **A**. **C**, confocal microscopic images of a tsA201 cell co-transfected with human YPet-AE1 and human CAII-CyPet. Comparison of **A** and **C** indicates that localization of mAE1 and hAE1 are identical. **D**, fluorescence control. The figure shows an overview over a patch of confluent tsA201 cells co-transfected with CAII-CyPet and YPet-AE1. Regions 1–4 represent non-transfected cells. Note the absence of non-specific fluorescence in the non-transfected cells, even with saturation of CyPet fluorescence (left panel). Non-saturated CyPet images were devoid of peripheral membrane enhancement (not shown). Arrows in right panel indicate morphologically unhealthy cells.

CAII-V143Y fusion protein on endogenous CA activity for the untagged CAII-V143Y protein: in this additional series of experiments expression of the CAII mutant reduced intracellular CA activity also by a similar 30% ($P < 0.001$, $n = 8$) and, associated with this, a $P_{\text{HCO}_3^-}$ decreased by $\sim 22\%$. This shows that a significant reduction of endogenous CAII expression is induced by expression of both tagged and untagged CAII-V143Y. Moreover, in preliminary experiments with HEK293 cells, we observe also in these cells a strong reduction of intracellular

CA activity when coexpressing hAE1-YPet together with CAII-V143Y-CyPet (own unpublished experiments). The rightmost data point in Fig. 6 (◆) represents tsA201 cells expressing the fusion protein with WT CAII (see Fig. S3A). This leads to increased intracellular CA activity in parallel with a statistically significantly increased HCO_3^- permeability ($5.6 \times 10^{-4} \text{ cm s}^{-1}$; $P < 0.01$). The third data point from the left in Fig. 6 (●) reflects tsA201 cells expressing the fusion protein containing N-terminally truncated CAII (see also Fig. S4A), which should not bind to the AE1 C-terminal cytoplasmic tail. This truncated CAII increased intracellular CA activity to the same level as did WT CAII, from ~ 800 to ~ 1000 . $P_{\text{HCO}_3^-}$ in the presence of truncated CAII is $4.9 \times 10^{-4} \text{ cm s}^{-1}$, significantly higher than control ($P < 0.05$). Note that the only modest increases in intracellular CA activity by expression of WT-CAII and of truncated CAII expression might result from a suppression of endogenous CAII similar to that observed with CAII-V143Y expression. In conclusion, in cells coexpressing AE1 with all tested CAII variants, the HCO_3^- permeabilities follow a regression line of $P_{\text{HCO}_3^-}$ rising moderately with increasing intracellular CA activity. The correlation coefficient of the linear regression of the data points in Fig. 6 is $r = 0.96$ and the slope of the regression line $\Delta P_{\text{HCO}_3^-} / \Delta A_i = 3.7 \times 10^{-7} \text{ cm s}^{-1}$ is statistically significantly different from zero ($P < 0.05$).

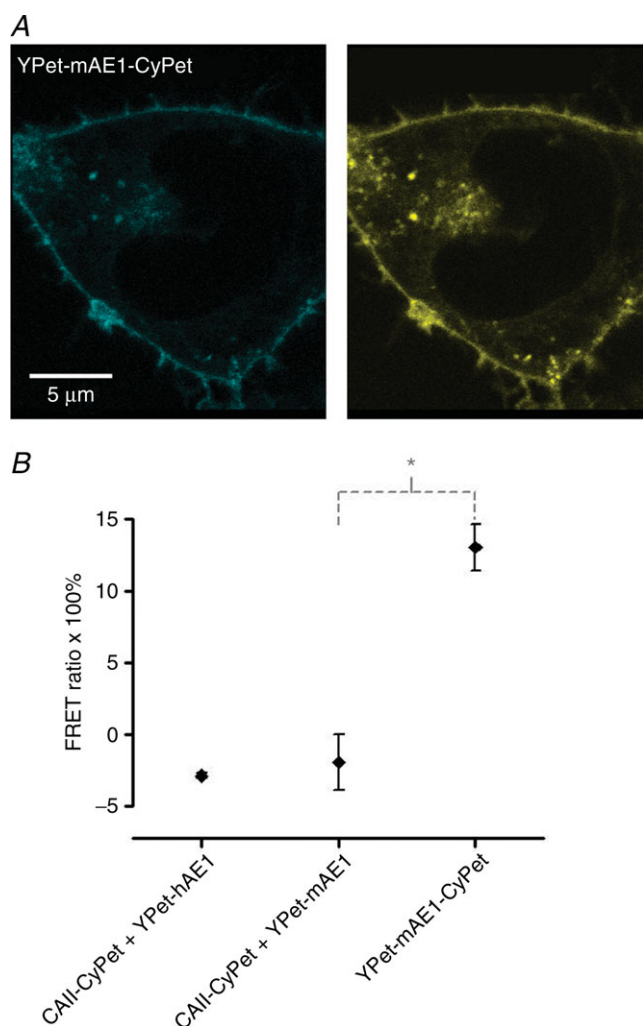


Figure 4. FRET measurements of CyPet- and YPet-labelled fusion proteins in tsA201 cells

A, confocal microscopic images of a tsA201 cell transfected with the doubly labelled construct of mAE1 N-terminally fused with YPet and C-terminally fused to CyPet. Illumination with 458 nm excites both CyPet (left) and YPet (right), the two dyes yielding an identical pattern. This construct gives the positive FRET signal seen in Fig. 5B. B, results of FRET experiments with tsA cells cotransfected with CAII-CyPet and YPet-hAE1 (left), with CAII-CyPet and YPet-mAE1 (centre), and a FRET control in cells transfected with YPet-mAE1-CyPet (right). This latter construct ensures proximity of the two dyes, reflected in its significantly positive FRET signal.

* $P < 0.01$ (t test); n from left to right is 3, 7 and 7. Bars represent SE values.

CA activity and $P_{\text{HCO}_3^-}$ in normal and CAII-deficient human RBCs

Here, we employ a different approach to test a functionally significant interaction between CAII and AE1, by examining red cells from two patients with homozygous CAII deficiency. Red cells in this disease lack all CAII activity, but maintain substantial erythroid CA activity due to the normal presence of CAI (Sly *et al.* 1983; Dodgson *et al.* 1988). While the intracellular CA activity of normal human RBCs at 37°C is 20,000 (Fig. 7A), in agreement with previous determinations (Endeward *et al.* 2008), the activity in RBCs from both patients is around 5000. Thus, erythroid CAI sustains 25% residual total erythroid CA activity, far in excess of that required for gas exchange at rest and with exercise (Dodgson *et al.* 1988). Figure 7B shows that the HCO_3^- permeabilities of normal and CAII-deficient RBCs are indistinguishable at $1.2\text{--}1.4 \times 10^{-4} \text{ cm s}^{-1}$, in agreement with previously reported normal values (Endeward *et al.* 2006, 2008). We conclude that AE1 transport activity in human RBCs is independent of the presence or absence of CAII activity. This complete lack of an effect of CAII on erythroid HCO_3^- transport may be compared with the moderate, albeit significant, effect of CAII expression in AE1-expressing tsA201 cells, which becomes apparent at a

much lower level of absolute CA activity values of ≤ 1000 (Fig. 6).

Mathematical simulation of the effect of CA on HCO_3^- uptake by red cells

These calculations were performed for the conditions of the human RBC, but in principle apply qualitatively to any CA-containing cell. Figure 8 portrays calculated time courses of HCO_3^- uptake at different intracellular CA activities. The time axis ends at 0.7 s, the capillary transit time in human lung and tissues. It is apparent that for the physiological intracellular CA activity of human RBCs of 20,000 (Fig. 7A), the process of erythroid HCO_3^- uptake is complete within the capillary transit time. Even for a CA activity of ~ 5000 , as observed in CAII-deficient RBCs, the capillary transit time suffices to reach completion of HCO_3^- uptake. However, below a CA activity of 1000 and extending to the complete absence of CA activity (equal to an acceleration factor of CO_2 hydration of 1), further deceleration of HCO_3^- uptake progressively decreases the total HCO_3^- influx achieved within the capillary transit time. The dependence of the process on CA activity is also reflected in the prediction by the mathematical model, 100 ms after initiation of HCO_3^- uptake, of a nearly linear gradient of intracellular pH_i (ΔpH_i of ~ 0.02 over the $0.8 \mu\text{m}$ half-thickness of the red cell) when $A_i = 20,000$ (with an average pH_i of 7.27), but of virtually no intra-

cellular pH gradient when $A_i = 1$ ($\text{pH}_i = 7.20$ everywhere in the cell). Across the range of CA activities between 1 and 1000, erythroid HCO_3^- uptake depends strongly on intracellular CA activity. Comparison of the initial rates of HCO_3^- uptake from curves with $A_i = 1$ and $A_i = 500$ in Fig. 8 reveals a >2 -fold increase, whereas the initial rates from slopes with $A_i = 5000$ and $A_i = 20,000$ show only minimal A_i dependence. It is clear from Fig. 8 that AE1-mediated HCO_3^- fluxes or permeabilities cannot be appraised without knowledge of intracellular CA activity.

Mathematical simulation of membrane HCO_3^- and CO_2 transport, with intracellular CA activity either homogeneously distributed in the cytoplasm or associated with the membrane

Again, these calculations were performed assuming conditions of the human RBC. The aim was to determine whether it makes a difference for the process of HCO_3^- or CO_2 uptake by red cells if total intracellular CA activity is (1) homogeneously distributed in the cytoplasm, as held by classical views, or (2) concentrated at the internal side of the membrane due to binding to membrane protein, as postulated for CAII by Vince and Reithmeier (1998). Figure 9A shows the result for HCO_3^- uptake by RBCs, when, starting from standard conditions of $p_{\text{CO}_2} = 40$ mmHg and extracellular pH (pH_e) of 7.40 at 37°C , the extracellular HCO_3^- concentration $[\text{HCO}_3^-]_e$ is

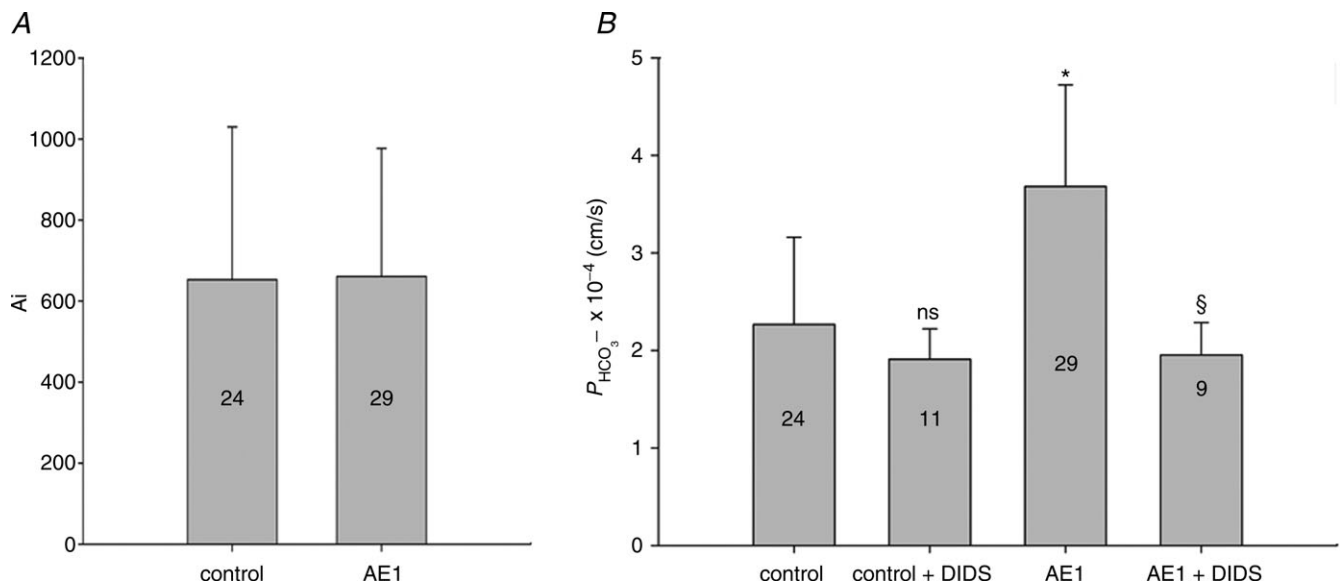


Figure 5. Carbonic anhydrase activity and HCO_3^- permeability in native and YPet-mAE1-expressing tsA201 cells

A, intracellular CA activities measured in lysates of untreated tsA201 cells (control) and tsA201 cells transfected with YPet-mAE1 (AE1), using the mass spectrometric ^{18}O technique. B, cellular $P_{\text{HCO}_3^-}$ measured in untreated tsA201 cells (control) and in tsA201 cells expressing YPet-mAE1 (AE1), in the absence or presence of DIDS (10^{-5} M), a strong inhibitor of AE1 transport function. DIDS showed no effect on $P_{\text{HCO}_3^-}$ of control cells, but inhibited the AE1-associated increase in $P_{\text{HCO}_3^-}$. ns, $P > 0.05$, * $P < 0.02$, § $P < 0.02$. Number of measurements are inside the columns. Error bars represent SD values.

subjected to a step increase from 25 to 35 mM. It is apparent that total absence of CA in the cell (the lowermost curve) leads to a drastic slowing of the process of HCO_3^- uptake, which after a rapid initial influx becomes extremely slow because the reaction required to convert HCO_3^- in the cell to CO_2 , thereby maintaining a significant driving force for HCO_3^- across the cell membrane, is uncatalysed. After a capillary transit time of 0.7 s, HCO_3^- uptake is far from completion, as also shown in Fig. 9A. If the normal

intra-erythrocytic CA activity of 20,000 is assumed to be homogeneously distributed in the cell interior (uppermost curve, in blue) HCO_3^- uptake is considerably accelerated and reaches completion after about 0.5 s. This is similar for the case when all CA activity of the cell is concentrated in a layer of $0.01 \mu\text{m}$ thickness ($1/80$ of $0.8 \mu\text{m}$) immediately adjacent to the internal side of the cell membrane (middle curve, in red). However, this latter condition does not

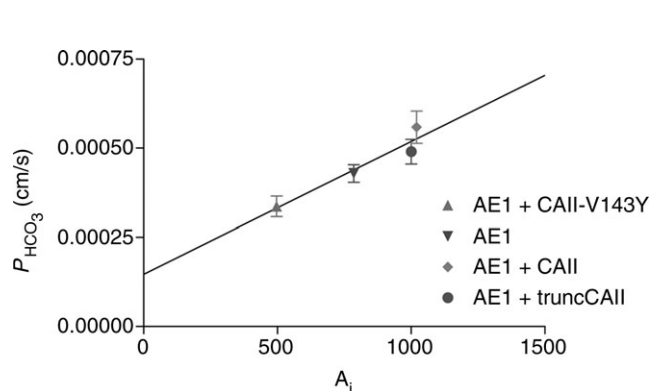


Figure 6. Bicarbonate permeability of tsA201 cells as a function of intracellular CA activity, A_i

tsA201 cells transfected with YPet-mAE1 ('control') (∇); tsA201 cells co-transfected with CAII-V143Y-CyPet and YPet-mAE1 (\triangle); co-transfection with WT CAII-CyPet and YPet-AE1 (\blacklozenge); co-transfection with N-terminally truncated CAII-CyPet and YPet-mAE1 (\bullet). Observed variations of $P_{\text{HCO}_3^-}$ are linearly related to intracellular CA activity. Correlation coefficient $r = 0.90$. Bars represent SE values. Number of determinations $n = 17, 18, 17$ and 33 (from left to right). All permeabilities under expression of the various CAII's are statistically significantly different from the mean control $P_{\text{HCO}_3^-}$ value (∇ , transfection with YPet-mAE1 only). P values between <0.01 and <0.05 .

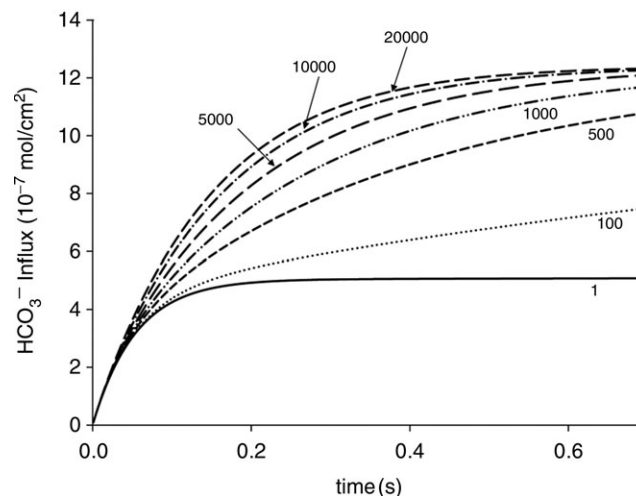


Figure 8. Time courses of bicarbonate influx, expressed as $\text{mol HCO}_3^- (\text{cm}^2 \text{ membrane surface area})^{-1}$, for various intra-erythrocytic CA activities, calculated with the model illustrated in Fig. S2 (upper scheme)

The numbers on the curves indicate the acceleration factors of CO_2 hydration. Therefore, 1 indicates the absence of CA activity, and 20,000 an activity of $(20,000 - 1)$. The dependence of HCO_3^- influx on CA activity is most pronounced between 1 and 1000, and becomes minor between 5000 and 20,000.

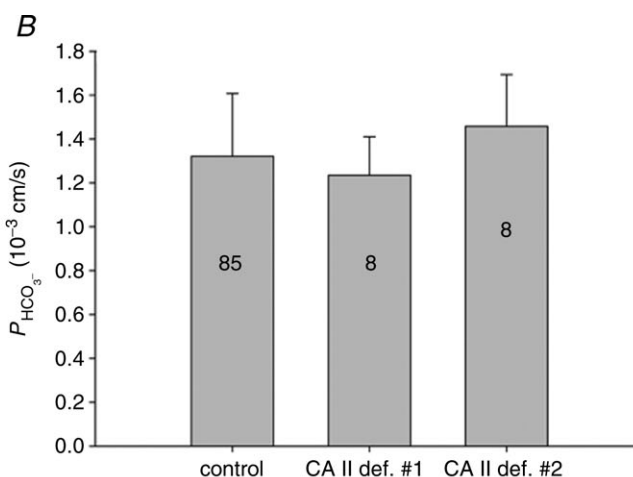
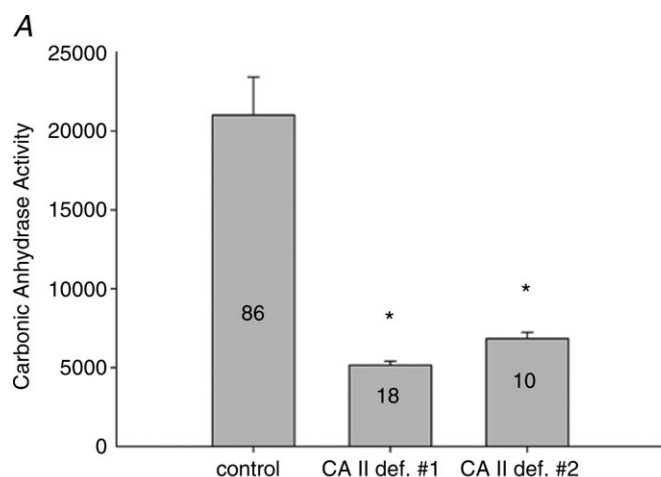


Figure 7. Intra-erythrocytic CA activity and bicarbonate permeability of normal (control) and CAII-deficient human red blood cells (the latter from two individuals 1 and 2)

A, while normal human red cells exhibit a CA activity of 20,000, CAII-deficient red cells have an activity of ~ 5000 due to the remaining CAI in these cells (* indicates statistically significant difference from control CA activity, $P < 0.01$). B, $P_{\text{HCO}_3^-}$ is identical regardless of whether CAII is present or completely absent. Numbers of measurements are given inside each column. Bars represent SD.

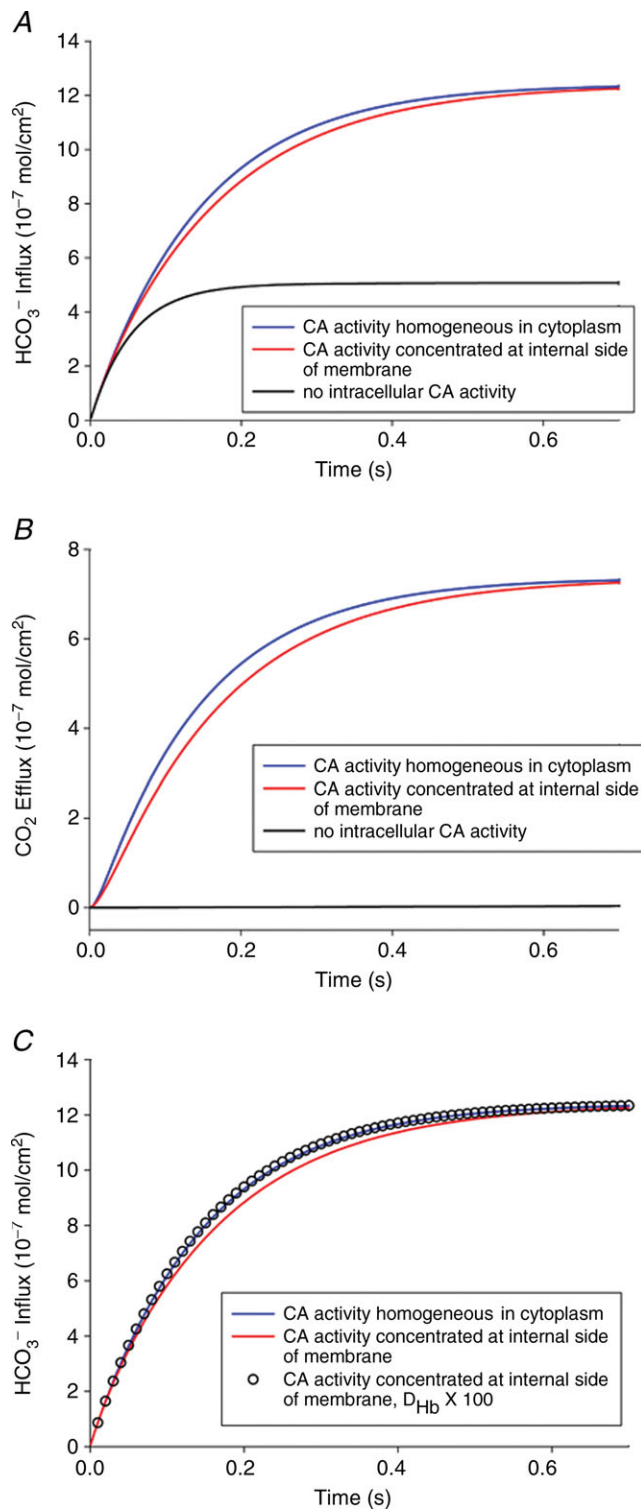


Figure 9. Significance of the subcellular localization of CA for uptake of HCO_3^- and the associated CO_2 release in human red cells

Uppermost curves (in blue): calculated for a homogeneous intracellular distribution of CA in the cytoplasm of red cells (upper scheme in Fig. S2). Middle curves (in red): calculated for an accumulation of all the CA of the red cell in a thin ($0.01 \mu\text{m}$) layer

lead to a faster HCO_3^- uptake compared with the homogeneously distributed CA activity, as might have been expected, but to a slightly slower one. In other words, it is somewhat more advantageous for HCO_3^- uptake to have the CA distributed all over the cell interior than to have it all very close to the membrane. Figure 9B illustrates the process of CO_2 efflux associated with HCO_3^- uptake, reflecting the amount of CO_2 leaving the cell after it has been produced by dehydration of the HCO_3^- taken up. The behaviour of the CO_2 efflux is a mirror image of that of the HCO_3^- influx: an extreme retardation in the absence of CA, and a slightly faster kinetics for homogeneously distributed CA than for a membrane-associated CA. We note that a distribution of the same total CA activity as used in the calculations of Fig. 9, split half-way between cytoplasmic and membrane-bound localization, produces curves intermediate between the middle and the uppermost curves of Fig. 9A and B.

Figure 9C serves to illustrate the mechanism responsible for the difference between the uppermost and middle curves in Fig. 9A and B. The curves represented by the open circles were calculated with the identical assumption underlying the middle curves of Fig. 9, namely accumulation of all intra-erythrocytic CA at the internal side of the membrane. However, the intracellular diffusion coefficient of haemoglobin was increased 100-fold above its actual value of $6.4 \times 10^{-8} \text{ cm}^2 \text{ s}^{-1}$, and as apparent from Fig. 9C, this causes the open circles to coincide with the uppermost curves. This shows that the relatively slow diffusion of intra-erythrocytic haemoglobin and thus the relatively slow intra-erythrocytic facilitated proton transport are responsible for a retardation of HCO_3^- uptake and CO_2 release when CA is concentrated at the internal side of the membrane rather than being, like haemoglobin, distributed homogeneously across the intracellular space (see Discussion).

immediately adjacent to the internal side of the red cell membrane (lower scheme in Fig. S2). Lowermost curves (black, in A and B): complete absence of CA activity inside a red cell. A, HCO_3^- influx after a step change in extracellular HCO_3^- from 25 to 35 mM. B, the efflux of CO_2 following the influx of HCO_3^- shown in A. C, effect of haemoglobin diffusivity on the kinetics of HCO_3^- exchange. The two curves are identical to the uppermost (blue) and middle (red) curves of A. The results represented by open circles were calculated for the accumulation of all red cell CA at the cytoplasmic side of the membrane, as in the lower (red) curve, with the exception that the diffusivity of haemoglobin was set to 100-fold its true value. This makes both types of CA distribution equivalent in terms of $\text{HCO}_3^-/\text{CO}_2$ exchange, indicating that intra-erythrocytic Hb-facilitated proton transport causes the limitation of the process when CA is associated with the membrane.

Discussion

CA supports membrane HCO_3^- transport most efficiently when it is homogeneously distributed in the cytoplasm

Figure 9 shows that a homogeneous presence of CA in the cytoplasm is predicted to be more favourable for uptake of HCO_3^- and release of CO_2 than restriction of intracellular CA to a 10 nm-thick layer immediately adjacent to the membrane. Although the latter situation guarantees that any HCO_3^- or CO_2 transferred across the membrane has instantaneous access to an extremely high CA activity, it nonetheless slows down the uptake process. This situation is reflected in the model calculation, which 100 ms after the start of HCO_3^- uptake shows in the immediate vicinity of the membrane a pH_i slightly higher when CA is concentrated at the membrane (7.28) than when CA is homogeneously distributed in the cytoplasm (7.27), and a 50% greater intracellular pH gradient of $\Delta\text{pH} = 0.03$ over $0.8 \mu\text{m}$ compared with the value under homogeneous CA distribution ($\Delta\text{pH} = 0.02$). Thus, in the former case protons right at the membrane are consumed somewhat more rapidly by the HCO_3^- dehydration reaction, but in the entire remainder of intracellular space the dehydration reaction is extremely slow and the development of the intracellular gradients of H^+ and HCO_3^- depends essentially on diffusion processes alone. A model in which the CA is partly concentrated at the membrane and partly distributed in the cytoplasm yields uptake curves intermediate between the middle and uppermost curves of Fig. 9, i.e. such a model is also inferior to that with homogeneous intracellular CA distribution. This result may appear counterintuitive. Indeed, the intuitive view that CA concentrated in the vicinity of the membrane should favour faster HCO_3^- transport has added to the great attractiveness of the metabolon concept. What is the reason for the contrary result? The answer is given in Fig. 9C, which shows that 100-fold acceleration of intracellular haemoglobin diffusion causes the difference in uptake kinetics between the two models to disappear. Since haemoglobin is the major intra-erythrocytic buffer, and its property of being a (mobile) buffer is its only function in the present model, this result leads to the following interpretation: when, for example, HCO_3^- has permeated the membrane and the catalysed dehydration reaction sets in, consuming protons to form CO_2 , the reaction can only continue as far as sufficient amounts of protons are available at the site where the reaction takes place. The available protons, however, are bound to the major buffer haemoglobin, and the haemoglobin is homogeneously distributed across the intra-erythrocytic space. Thus, delivery of protons from the cell interior towards the membrane region by haemoglobin-facilitated H^+ diffusion becomes rate-limiting, as free diffusion of

cytosolic protons is negligible at the low intracellular H^+ concentration. The slow diffusion of haemoglobin inside the red cell is also slow in comparison with the rates of other components of the uptake process (Moll, 1966; Gros & Moll, 1972, 1974; Junge & McLaughlin, 1987). If haemoglobin diffusion were 100 times faster, this limitation would not exist. Note that this problem is not restricted to RBCs, but applies to all cells, because the total H^+ buffer capacity in most cells reaches 30–50% that of RBCs, although the average buffer mobility is somewhat greater (Vaughan-Jones *et al.* 2002; Zaniboni *et al.* 2003; Swietach & Vaughan-Jones, 2005; Swietach *et al.* 2005, 2010). We conclude that for all cells, colocalization of CA with the major buffers maximizes rates of HCO_3^- transport. This situation applies when both are distributed homogeneously in the cytoplasm. This requires HCO_3^- (in the case of AE1-mediated HCO_3^- uptake, with HCO_3^- diffusion tightly coupled to oppositely directed diffusion of Cl^-) to diffuse to the locations of buffer and CA. These diffusion processes are much faster than facilitated proton transport because both HCO_3^- and Cl^- have rather high intracellular diffusivities (see Methods). The following illustrative example assumes identical concentration gradients of HCO_3^- and buffered protons. These intracellular concentration gradients must be identical due to the 1:1 stoichiometry of the reaction of H^+ and HCO_3^- . However, the gradients have opposite signs because, in the given example, we look either at the diffusion of HCO_3^- from the membrane into the cell interior (CA homogeneously distributed in the cytoplasm), or, alternatively, at the diffusional transport of protons from the cell interior towards the membrane (CA concentrated at the internal side of the membrane). In both cases, electroneutrality of these intracellular ion fluxes will be maintained by the intracellular Cl^- fluxes required to maintain the Hamburger shift. With an arbitrarily chosen concentration difference of 5 mM for both HCO_3^- and bound protons (the free H^+ being negligible), the products of diffusion coefficients and concentration gradients then are

$$\begin{aligned} \text{for } \text{H}^+ : D_{\text{Hb}} \cdot \text{BF} \cdot \Delta\text{pH} &= -6.4 \times 10^{-8} \text{ cm}^2 \text{ s}^{-1} \cdot 5 \text{ mM} \\ &= -3.2 \times 10^{-7} \text{ cm}^2 \text{ mM s}^{-1} \end{aligned}$$

for

$$\begin{aligned} \text{HCO}_3^- : D_{\text{HCO}_3^-} \cdot \Delta[\text{HCO}_3^-] &= 0.6 \times 10^{-5} \text{ cm}^2 \text{ s}^{-1} \cdot 5 \text{ mM} \\ &= 3 \times 10^{-5} \text{ cm}^2 \text{ mM s}^{-1}. \end{aligned}$$

HCO_3^- diffusion inside cells – and similarly Cl^- diffusion – thus is two orders of magnitude faster than proton transport. We note that an entirely analogous consideration applies to the process of CO_2 uptake, where CO_2 diffusion into the cell interior is much faster than proton transport into the cell interior. This fact makes it more efficient for the cell to localize the CA to the site(s) of optimal buffering.

Neither CAII colocalization with AE1 nor FRET signal attributable to an AE1–CAII interaction is detectable in CAII-expressing tsA201 cells

No subcellular localization studies of intact non-erythroid cells coexpressing AE1 and CAII have been reported to date. In Figs 3, 4 and S4 we present clear evidence that the fluorescent fusion proteins WT human CAII, N-terminally truncated CAII and the acatalytic V143Y CAII are all distributed homogeneously across the cytoplasm of transfected tsA201 cells. Qualitatively as well as quantitatively, the CAII fluorescence intensities show no accumulation of either CAII variant in the vicinity of the membrane. In contrast, fluorescent human and murine AE1 fusion proteins clearly colocalize with the cell surface membranes (with a small fraction of AE1 associated with intracellular vesicular structures). This clear result is confirmed by the absence of a FRET signal arising from coexpressed CyPet-labelled CAII and YPet-labelled human or murine AE1, whereas a doubly labelled AE1 provides a strong positive FRET signal. Thus, the present morphological studies show no evidence for physical association between CAII and AE1 within a distance of 8–10 nm. Note that the present fusion proteins have a molecular weight around 27 kDa greater than the native proteins CAII (29 kDa) and AE1 (~100 kDa). This could in principle disturb a close interaction of the two proteins. For this reason the dyes were attached to the C terminus of CAII and the N terminus of AE1, whereas the sites proposed to interact are the N terminus of CAII and the C terminus of AE1, in the hope of minimizing potential steric hindrance to the postulated interaction. For the case of CAII, a suppression of AE1–CAII interaction by the fluorophore attached to CAII can be ruled out by the finding described above that fluorophore-tagged and untagged CAII–V143Y reduce $P_{\text{HCO}_3^-}$ in the same way. A further strong argument against a CAII–AE1 complex in the present cell model is the absence of CAII–AE1 co-immunoprecipitation, in which native CAII and AE1 tagged at the N terminus with the small 2.7 kDa Flag were studied. We conclude that the two heterologous proteins in the present expression model do not form a physical complex at the plasma membrane.

Vince and Reithmeier (1998) investigated red cell ghosts washed only once, i.e. mildly in comparison with earlier studies (Tappan, 1968; Rosenberg & Guidotti, 1968; Randall & Maren, 1972). Immunofluorescence imaging of smears of these pink ghosts revealed both CAII and AE1 homogeneously distributed across the ghosts. Upon treatment with the AE1-binding tomato lectin to promote clustering of AE1, they observed clustering of both AE1 and CAII. Since the authors did not co-stain with antibodies to both AE1 and CAII, co-localization of the two proteins in the clusters was not definitively shown. On the other hand, Campanella *et al.* (2005) observed co-localization of AE1 and CAII by confocal immuno-

fluorescence analysis of intact human RBCs fixed in 0.5% acrolein and subsequently permeabilized in 0.1% Triton. Whereas AE1 immunostaining of the red cell membrane was continuous, CAII immunostaining was consistently punctate, and did not entirely coincide with that of AE1. The authors did not exclude the possibility of a fixation artifact, especially as more aggressive fixation promoted restriction to the cell periphery even of haemoglobin staining. This latter result was tentatively explained by binding of denatured or oxidized haemoglobin to the AE1 N terminus. Thus, additional approaches to assess CAII localization in intact red cells would be useful.

Lack of evidence for a functional metabolon of CAII and AE1 in tsA201 cells

Figure 8 shows clearly that calculated HCO_3^- uptake rate by cells, as when induced by an extracellular step change in HCO_3^- or Cl^- concentration and observed by an intracellular pH dye, depends very strongly on intracellular CA activity. This dependency is most pronounced in the CA activity range between 0 and ~1000, exactly the activity range of cell lines such as HEK293, tsA201 or MDCK cells. Therefore, valid comparisons of HCO_3^- fluxes between cells in which various CAII constructs are expressed can be made only if the intracellular CA activity is carefully controlled. These controls have often been missing in the literature reporting such flux measurements.

The present method of measuring HCO_3^- permeability differs from this classical type of experimental approach. We estimate $P_{\text{HCO}_3^-}$ by observing the exchange of ^{18}O between CO_2 , HCO_3^- and H_2O under conditions of perfect chemical – but not isotopic – equilibrium (Endeward & Gros, 2005; Endeward *et al.* 2006). The moderate dependency of $P_{\text{HCO}_3^-}$ on A_i that we see in Fig. 6 is due to the fact that the calculation of $P_{\text{HCO}_3^-}$ from ^{18}O exchange measurements assumes perfect stirring of the intracellular space (Endeward & Gros, 2005). As we have shown previously (Endeward & Gros, 2009), this is of course not realistic and the lack of intracellular mixing causes a delay in the cellular uptake of the substance considered, due to a build-up of the substance transferred into the cell at the internal side of the membrane. For CO_2 and HCO_3^- , this delay is diminished with increasing intracellular CA activity, which promotes inter-conversion between CO_2 and HCO_3^- , thus reducing the build-up of CO_2 or HCO_3^- at the membrane and accelerating the respective fluxes. As a consequence, slightly increasing HCO_3^- fluxes and slightly increasing $P_{\text{HCO}_3^-}$ are expected to parallel increases in A_i , as evident in Fig. 6 between CA activities of 500 and 1000. Between CA activities of 5000 and 20,000, such an effect is no longer visible (Fig. 7), consistent with prediction (Fig. 8).

From expression of the three types of CAII constructs in tsA201 cells, the following conclusions can be drawn from Fig. 6:

1. WT CAII. Expression of heterologous wild-type CAII fusion protein (◆) increases A_i over that in the mere presence of endogenous CAII (▼), and in parallel causes a moderate but significant increase in $P_{\text{HCO}_3^-}$ ($P < 0.01$). This could potentially be compatible with increased concentration of an AE1–CAII metabolon. However, in view of the general dependence of $P_{\text{HCO}_3^-}$ on A_i , such an explanation is not required. The fact that in the present study expression of WT CAII has a noticeable effect on $P_{\text{HCO}_3^-}$ is at variance with the report by Sterling *et al.* (2001a,b), who found no effect of WT CAII expression in HEK293 cells, and proposed that the endogenous CAII activity of HEK293 cells is sufficient for a full metabolon effect. The cause of this discrepancy with the present results is not clear, but does not affect the current finding that $P_{\text{HCO}_3^-}$ is positively and linearly related to A_i (Fig. 6).

2. Acatalytic CAII. Expressing the (almost) acatalytic CAII mutant V143Y fusion protein decreases endogenous CA activity from ~800 to ~480. This pronounced effect causes a reduction in $P_{\text{HCO}_3^-}$, which follows the general dependency of $P_{\text{HCO}_3^-}$ on A_i seen in Fig. 6. The metabolon hypothesis predicts that the V143Y mutant displaces some of the catalytically active native CAII from its binding site at AE1 to reduce transport activity. Indeed, Sterling *et al.* (2001a,b) observed that expression of CAII-V143Y reduced HCO_3^- transport rate by 40–60%. Similarly, Sowah and Casey (2011) observed substantial reduction of HCO_3^- transport activity of AE1 protein expressed in HEK293 cells with coexpression in the same cell of increasing levels of CAII-V143Y. In contrast, expression of the fusion protein AE1.CAII, instead of AE1, greatly reduced the inhibitory effect of CAII-V143Y expression, presumably because this fusion protein ensured the maintenance of a reasonably high CA activity inside these cells, although confined to the internal side of the cell membrane. Comparing the present expression of CAII-V143Y (Fig. S3b) with the immunoblots of Sterling *et al.* (2001a), it appears likely that expression of the mutant CAII protein was stronger in some of their experiments than in the present ones. The maximum amount of cDNA used by Sterling *et al.* (2001a) per unit of culture dish area was about twice as much as the amount of cDNA routinely used in this study. In addition, the transfection efficiency achieved by these authors may have exceeded that in the experiments presented here. On the other hand, even with the present modest transfection efficiencies of 30–40%, expression of V143Y-CAII reduces average intracellular CA activity from 800 to 480. Thus, expression of this mutant is associated with a marked reduction of endogenous CAII activity in the transfected cells. Our observation that untagged CAII-V143Y causes a similar reduction of endogenous CA as that caused

by the tagged construct supports the possibility that in Sterling's (2001a) experiments the expression of untagged CAII-V143Y may have resulted in a similarly decreased intracellular CA activity. As mentioned above, our preliminary results show that marked decreases in intracellular CA activity upon expression of heterologous AE1 and CAII-V143Y can also be found in HEK293 cells. The mechanism by which AE1 activity was reduced in the experiments of Sterling *et al.* (2001a,b) and of Sowah and Casey (2011) might then have been a marked reduction in intracellular CA activity rather than the proposed displacement of endogenous CAII from its AE1 binding site by the V143Y mutant. We note that, as apparent from Fig. 5A, expression of the AE1 fusion protein appears not to affect endogenous CAII activity. Conversely, variation of exogenous CAII-V143Y expression was shown by Sterling *et al.* (2001a,b) and Sowah and Casey (2011) to have no suppressive effect on the expression of AE1 in HEK293 cells. Thus, while expression of exogenous CAII-V143Y – and possibly that of exogenous WT-CAII as well – interferes with expression of endogenous CAII, expression of AE1 and CAII do not seem to interfere with each other. Consistent with this, in the experiments of Sowah and Casey (2011) expression of CAII-V143Y did not alter expression of either WT AE1 or of the fusion protein AE1.CAII, a modified AE1 membrane protein. In the case of the AE1.CAII fusion protein, AE1 transport activity was fairly well maintained under CAII-V143Y expression, presumably due to the unaffected activity of the AE1-fused CAII (see fig. 3B in their paper) and despite a likely reduction in endogenous cytosolic CAII expression. In conclusion, expression of exogenous CAII-V143Y does not seem to impair expression of AE1 membrane protein, so this is not likely to be the mechanism of the observed reductions of AE1 transport activity. Rather, we suggest that the present results, and perhaps those of Sterling *et al.* (2001a) and Sowah and Casey (2011), reflect the reduced intracellular CA activity during CAII-V143Y expression. Thus, the dependence of AE1 activity on CAII-V143Y expression can be explained without invoking a functionally important AE1–CAII metabolon in transfected tsA201 cells, and probably in transfected HEK293 cells as well.

3. N-terminally truncated CAII. Another striking finding illustrated in Fig. 6 in terms of the metabolon hypothesis is the expression of truncated CAII, which lacks the proposed binding site of CAII to AE1. This expression leads to an A_i increase from 800 to 1000 (similar to the increased activity that accompanies expression of WT-CAII), and in parallel moderately but significantly increases $P_{\text{HCO}_3^-}$ ($P < 0.05$). The *in vitro* assays of Vince *et al.* (2000) showed that the truncated CAII does not bind to AE1. Unfortunately, measurements of the effect of expression of truncated CAII on HCO_3^- transport have not previously been reported. The metabolon concept

predicts simply that expression of the truncated CAII would not compete with endogenous CAII for the AE1 binding site, and thus would not alter AE1 transport activity. Instead, we observe a significant increase in $P_{\text{HCO}_3^-}$, again consistent with the direct relationship between $P_{\text{HCO}_3^-}$ and intracellular CA activity.

Sterling *et al.* (2001*a,b*) also reported that AE1 mutants, in which the C-terminal binding motif for CAII was changed or deleted, exhibited a 90% reduction of transport activity when expressed in HEK293 cells. However, preservation of the intrinsic transport activity of these mutants in the absence of CAII was not studied, so these experiments were not entirely conclusive. Specifically, Sterling *et al.* (2001*a,b*) reported that the C-terminal missense mutation LDADD→LAAAA led to nearly complete loss of HCO_3^- transport activity of hAE1 in the presence of endogenous CAII activity in HEK293 cells. Later, Dahl *et al.* (2003) studied in kidney AE1 the same LDADD→LAAAA mutation which, when expressed in *Xenopus* oocytes, exhibited normal Cl^-/Cl^- self-exchange activity but almost completely suppressed $\text{Cl}^-/\text{HCO}_3^-$ exchange activity, with or without coexpressed CAII (note that native *Xenopus* oocytes express negligible levels of intracellular CA activity; Nakhoul *et al.* 1996, 1998; Becker & Deitmer, 2007, 2008). This might indicate that missense mutations in the region of the LDADD motif can eliminate intrinsic $\text{Cl}^-/\text{HCO}_3^-$ transport activity independently of the presence or absence of CAII, while at the same time leaving Cl^-/Cl^- self-exchange activity unaffected. This scenario could also explain the above cited result of Sterling *et al.* (2001*a,b*).

HCO_3^- permeability of CAII-deficient red cells is identical to that of normal red cells

The CAII-deficient RBCs from two different patients were free of CAII activity as reported in the original description of this syndrome (Sly *et al.* 1983) and in a later review (Shah *et al.* 2004). However, as reported previously (Dodgson *et al.* 1988) and shown in Fig. 7A, the substantial residual CAI activity of these cells is more than sufficient for the requirements of capillary CO_2 exchange in lung and tissues (Swenson & Maren, 1978). It can thus be expected that the processes of HCO_3^- and CO_2 uptake by CAII-deficient red cells are minimally impaired compared with those of normal RBCs. This is demonstrated in Fig. 8, which applies the mathematical model described above to illustrate the effect of different cytoplasmic CA activities on the kinetics of HCO_3^- uptake. It is apparent that varying intracellular CA activities between 5000 (as in CAII-deficient RBCs) and 20,000 (as in normal RBCs) is of minimal consequence to HCO_3^- uptake kinetics.

Thus, the CAII-deficient human red cell appears to be an ideal model in which to study the question of whether CAII affects HCO_3^- permeation across the cell

membrane: it retains substantial CA activity from its residual CAI, but lacks the proposed ability of CAII to bind to AE1 (Vince & Reithmeier, 1998). As seen in Fig. 7B, the HCO_3^- permeabilities measured for normal and CAII-deficient RBCs are indistinguishable. These values of $P_{\text{HCO}_3^-}$ calculated from the mass spectrometric records use the correct respective intracellular CA activities as described previously (Endeward & Gros, 2005; Endeward *et al.* 2008). Figure 7B shows that absence of CAII does not affect HCO_3^- permeation, and thus CAII in human red cells has no functional effect on HCO_3^- transport by AE1. HCO_3^- uptake would slow down considerably if intra-erythrocytic CA activity were to decrease below about 1000, as indicated in Fig. 8, but this is a general effect of the speed of the intracellular hydration–dehydration reaction, and reflects no specific direct effect of CAII on AE1.

Conclusion

The present study investigates the AE1–CAII metabolon hypothesis by a variety of approaches. First, we study by an elaborate theoretical model which level of intracellular CA activity is required to abolish limitation of the rate of uptake or release of HCO_3^- by cells by the intracellular speed of hydration–dehydration. This CA activity is roughly between 1000 and 5000. Since many cell lines have CA activities below 1000, it is to be expected that in cells used for expression of AE1, the speed of HCO_3^- transport is often limited by their intracellular CA activity. This is also the case in the results reported here, which show a moderate increase in $P_{\text{HCO}_3^-}$ of tsA201 cells with intracellular CA activity increasing from 500 to 1100. We find that expression of the acatalytic CAII mutant V143Y reduces $P_{\text{HCO}_3^-}$, that additional expression of WT CAII increases $P_{\text{HCO}_3^-}$ and that expression of an N-terminally truncated CAII lacking the proposed AE1 binding region also increases $P_{\text{HCO}_3^-}$. All these changes in $P_{\text{HCO}_3^-}$ can be attributed to corresponding changes in intracellular CA activity. Thus, none of these experiments suggests a required specific interaction of AE1 and CAII as proposed in the metabolon hypothesis. These data are strongly supported by the fact that CAII-deficient human RBCs exhibit a HCO_3^- permeability identical to that of normal human red cells. The CAII-deficient red cells have sufficiently high intracellular CA activity (due to residual CAI that lacks a known AE1 binding motif) to ensure a HCO_3^- transport rate not limited by the speed of the CO_2 hydration–dehydration reaction. Thus, the present results offer no evidence of a functionally important physical interaction of CAII and AE1. Studies expressing YPet and CyPet-labelled human CAII and human or murine AE1 in tsA201 cells show no colocalization of CAII with AE1 at the cell membrane. This result is further supported by the absence of a FRET signal, indicating that CAII and AE1 in

the cell are separated by distances greater than 8–10 nm, i.e. they do not form a complex. Similarly, we find no co-immunoprecipitation of native CAII and Flag-tagged AE1 expressed in tsA201 cells. As a further interesting piece of evidence, the theoretical model presented here shows that it is more effective for transmembrane HCO_3^- (and CO_2) transport to have the cellular CA homogeneously distributed across the cytoplasm, for the major reason that the cellular buffers are also distributed all over the cell interior, thereby ensuring that H^+ produced or consumed by the CA-mediated reactions have immediate access to these buffers. Thus, the actual and also the most favourable localization of CAII within cells in terms of AE1 transport activity appears to be a homogeneous distribution throughout the cell interior.

Other HCO_3^- transporters than AE1 have been reported to possess the binding motif suggested to bind to CAII and to form a metabolon with CAII, similar to that with AE1: the sodium HCO_3^- cotransporters NBC1 and NBC3 and the human putative anion transport 1, SLC26A6/PAT-1 (Gross *et al.* 2002; Alvarez *et al.* 2003; Loisel *et al.* 2004). In addition, a substantial – although controversial – body of evidence has been presented to show that CAII can be either pulled down with recombinant fragments of SLC4 proteins or fusion proteins or co-immunoprecipitates with intact SLC4 protein (Gross *et al.* 2002; McMurtrie *et al.* 2004; Pushkin *et al.* 2004; Alvarez *et al.* 2005; Lu *et al.* 2006; Boron, 2010; Yamada *et al.* 2011). Additional biochemical and suggestive genetic data have been presented for transport metabolons in bacteria and other organisms (Moraes & Reithmeier, 2012). Our data do not allow us to draw any inferences as regards these proposed metabolons. It should be noted, however, that recently Schueler *et al.* (2011) have reported that CAI, which lacks the binding region proposed to mediate the binding between all these transporters and CAII, clearly increases NBCe1 transport activity. These authors show that the major determinant of NBCe1 transport activity appears to be the level of intracellular CA catalytic activity, independent of the CA isoform responsible for this activity. This conclusion is entirely in line with the main conclusion of the present study on AE1 transport properties.

References

- Alvarez BV, Loisel FB, Supuran CT, Schwartz GJ & Casey JR (2003). Direct extracellular interaction between carbonic anhydrase IV and the human NBC1 sodium/bicarbonate co-transporter. *Biochemistry* **28**, 12321–12329.
- Alvarez BV, Vilas GL & Casey JR (2005). Metabolon disruption: a mechanism that regulates bicarbonate transport. *EMBO J* **24**, 2499–2511.
- Becker HM & Deitmer JW (2007). Carbonic anhydrase II increases the activity of the human electrogenic $\text{Na}^+/\text{HCO}_3^-$ cotransporter. *J Biol Chem* **282**, 13508–13521.
- Becker HM & Deitmer JW (2008). Nonenzymatic proton handling by carbonic anhydrase II during H^+ -lactate cotransport via monocarboxylate transporter 1. *J Biol Chem* **283**, 21655–21667.
- Bennett V & Stenbuck PJ (1979). The membrane attachment protein for spectrin is associated with band 3 in human erythrocyte membranes. *Nature* **280**, 468–473.
- Boron WF (2010). Evaluating the role of carbonic anhydrases in the transport of HCO_3^- related species. *Biochim Biophys Acta* **1804**, 410–421.
- Campanella ME, Chu H & Low PS (2005). Assembly and regulation of a glycolytic enzyme complex on the human erythrocyte membrane. *Proc Natl Acad Sci U S A* **102**, 2402–2407.
- Dahl NK, Jiang L, Chernova MN, Stuart-Tilley AK, Shmukler BE & Alper SE (2003). Deficient HCO_3^- transport in an AE1 mutant with normal Cl^- transport can be rescued by carbonic anhydrase II presented on an adjacent AE1 protomer. *J Biol Chem* **278**, 44949–44958.
- Dodgson SJ, Forster RE, Sly WS & Tashian RE (1988). Carbonic anhydrase activity of intact carbonic anhydrase II-deficient human erythrocytes. *J Appl Physiol* **65**, 1472–1480.
- Endeward V, Cartron JP, Ripoché P & Gros G (2008). RhAG protein of the Rhesus complex is a CO_2 channel in the human red cell membrane. *FASEB J* **22**, 64–73.
- Endeward V & Gros G (2005). Low carbon dioxide permeability of the apical epithelial membrane of guinea-pig colon. *J Physiol* **567**, 253–265.
- Endeward V & Gros G (2009). Extra- and intracellular unstirred layer effects in measurements of CO_2 diffusion across membranes – a novel approach applied to the mass spectrometric ^{18}O technique for red blood cells. *J Physiol* **587**, 1153–1167.
- Endeward V, Musa-Aziz R, Cooper GJ, Chen LM, Pelletier MF, Virkki LV, Supuran CT, King LS, Boron WF & Gros G. (2006). Evidence that aquaporin 1 is a major pathway for CO_2 transport across the human erythrocyte membrane. *FASEB J* **20**, 1974–1981.
- Enns T (1967). Gas transport and the red cell. *Fed Proc* **26**, 1802–1804.
- Fierke CA, Calderone TL & Krebs JF (1991). Functional consequences of engineering the hydrophobic pocket of carbonic anhydrase II. *Biochemistry* **30**, 11054–11063.
- Forster RE (1964). Rate of gas uptake by red cells. In *Handbook of Physiology*, Section 3, *Respiration*, vol. 1, eds Fenn WO & Rahn H. The American Physiological Society, Washington, DC. chapter 32, pp. 827–837.
- Geigy JR (1960). *Documenta Geigy Wissenschaftliche Tabellen*, 6th edn. Geigy, Basel.
- Gros G & Moll W (1972). The facilitated diffusion of CO_2 in hemoglobin solutions and phosphate solutions. In *Oxygen Affinity of Hemoglobin and Red Cell Acid Base Status*, eds Rørth M & Astrup P. Munksgaard-Academic Press, Copenhagen, pp. 484–492.
- Gros G & Moll W (1974). Facilitated diffusion of CO_2 across albumin solutions. *J Gen Physiol* **64**, 356–371.
- Gros G, Moll W, Hoppe H & Gros H (1976). Proton transport by phosphate diffusion – a mechanism of facilitated CO_2 transfer. *J Gen Physiol* **67**, 773–790.

- Gross E, Pushkin A, Abuladze N, Fedotoff O & Kurtz I (2002). Regulation of the sodium bicarbonate cotransporter kNBC1 function: role of Asp⁹⁸⁶, Asp⁹⁸⁸ and kNBC1-carbonic anhydrase II binding. *J Physiol* **544**, 679–685.
- Hu PY, Roth DE, Skaggs LA, Venta PJ, Tashian RE, Guibaud P & Sly WS (1992). A splice junction mutation in intron 2 of the carbonic anhydrase II gene of osteopetrosis patients from Arabic countries. *Hum Mutat* **1**, 288–292.
- Itel F, Al-Samir S, Öberg F, Chami M, Kumar M, Supuran CT, Deen PM, Meier W, Hedfalk K, Gros G & Endeward V (2012). CO₂ permeability of cell membranes is regulated by membrane cholesterol and protein gas channels. *FASEB J* **26**, 5182–5191.
- Itada N & Forster RE (1977). Carbonic anhydrase activity in intact red blood cells measured with ¹⁸O exchange. *J Biol Chem* **252**, 3881–3890.
- Junge W & McLaughlin S (1987). The role of fixed and mobile buffers in the kinetics of proton movement. *Biochim Biophys Acta* **890**, 1–5.
- Kifor G, Toon MR, Janoshazi A & Solomon AK (1993). Interaction between red cell membrane band 3 and cytosolic carbonic anhydrase. *J Membr Biol* **134**, 169–179.
- Loiselle FB, Morgan PE, Alvarez BV & Casey JR (2004). Regulation of the human NBC3 Na⁺/HCO₃[−] cotransporter by carbonic anhydrase II and PKA. *Am J Physiol Cell Physiol* **286**, C1423–1433.
- Lu J, Daly CM, Parker MD, Gill HS, Piermarini PM, Pelletier MF & Boron WF (2006). Effect of human carbonic anhydrase II on the activity of the human electrogenic Na/HCO₃ cotransporter NBCe1-A in *Xenopus* oocytes. *J Biol Chem* **281**, 19241–19250.
- McMurtrie HL, Cleary HJ, Alvarez BV, Loiselle FB, Sterling D, Morgan PE, Johnson DE & Casey JR (2004). The bicarbonate transport metabolon. *J Enzyme Inhib Med Chem* **19**, 231–236.
- Michael P & Bennett V (1995). The ANK repeats of erythrocyte ankyrin form two distinct but cooperative binding sites for the erythrocyte anion exchanger. *J Biol Chem* **270**, 22050–22057.
- Moll W (1966). The diffusion coefficient of haemoglobin. *Respir Physiol* **1**, 357–365.
- Moraes TF, Reithmeier RA (2012). Membrane transport metabolons. *Biochim Biophys Acta* **1818**, 2687–2706.
- Nakhoul NL, Davis BA, Romero MF & Boron WF (1998). Effect of expressing the water channel aquaporin-1 on the CO₂ permeability of *Xenopus* oocytes. *Am J Physiol* **274**, C543–C548.
- Nakhoul NL, Romero MF, Waheed A, Davis BA, Mullins R, Hageman G, Sly WS & Boron WF (1996). Processing and functional expression of carbonic anhydrase isoforms in *Xenopus laevis* oocytes (Abstract). *FASEB J* **10**, A88.
- Nguyen AW & Daugherty PS (2005). Evolutionary optimization of fluorescent proteins for intracellular FRET. *Nat Biotechnol* **23**, 355–360.
- Papadopoulos S, Leuranguer V, Bannister RA & Beam KG (2004). Mapping sites of potential proximity between the dihydropyridine receptor and RyR1 in muscle using a cyan fluorescent protein–yellow fluorescent protein tandem as a fluorescence resonance energy transfer probe. *J Biol Chem* **279**, 44046–44056.
- Parkes JL & Coleman PS (1989). Enhancement of carbonic anhydrase activity by erythrocyte membranes. *Arch Biochem Biophys* **275**, 459–468.
- Piermarini PM, Kim EY & Boron WF (2007). Evidence against a direct interaction between intracellular carbonic anhydrase II and pure C-terminal domains of SLC4 bicarbonate transporters. *J Biol Chem* **282**, 1409–1421.
- Pushkin A, Abuladze N, Gross E, Newman D, Tatishchev S, Lee I, Fedotoff O, Bondar G, Azimov R, Nguyen M & Kurtz I (2004). Molecular mechanism of kNBC1-carbonic anhydrase II interaction in proximal tubule cells. *J Physiol* **559**, 55–65.
- Randall RF & Maren TH (1972). Absence of carbonic anhydrase in red cell membranes. *Biochim Biophys Acta* **268**, 730–732.
- Rosenberg SA & Guidotti G (1968). The protein of human erythrocyte membranes. I. Preparation, solubilization, and partial characterization. *J Biol Chem* **243**, 1985–1992.
- Schueler C, Becker HM, McKenna R & Deitmer JW (2011). Transport activity of the sodium bicarbonate cotransporter NBCe1 is enhanced by different isoforms of carbonic anhydrase. *PLoS ONE* **6**, e27167.
- Shah GN, Bonapace G, Hu PY, Strisciuglio P & Sly WS (2004). Carbonic anhydrase II deficiency syndrome (osteopetrosis with renal tubular acidosis and brain calcification): novel mutations in CA2 identified by direct sequencing expand the opportunity for genotype–phenotype correlation. *Hum Mutat* **24**, 272.
- Sly WS, Hewett-Emmett D, Whyte MP, Yu YS & Tashian RE (1983). Carbonic anhydrase II deficiency identified as the primary defect in the autosomal recessive syndrome of osteopetrosis with renal tubular acidosis and cerebral calcification. *Proc Natl Acad Sci U S A* **80**, 2752–2756.
- Sowah D & Casey JR (2011). An intramolecular transport metabolon: fusion of carbonic anhydrase II to the COOH terminus of the Cl[−]/HCO₃[−] exchanger, AE1. *Am J Physiol Cell Physiol* **301**, C336–C346.
- Sterling D, Reithmeier RA & Casey JR (2001a). A transport metabolon. Functional interaction of carbonic anhydrase II and chloride/bicarbonate exchangers. *J Biol Chem* **276**, 47886–47894.
- Sterling D, Reithmeier RA & Casey JR (2001b). Carbonic anhydrase: in the driver's seat for bicarbonate transport. *J Pancreas* **2**, 165–170.
- Swenson ER & Maren TH (1978). A quantitative analysis of CO₂ transport at rest and during maximal exercise. *Respir Physiol* **35**, 129–159.
- Swietach P, Leem CH, Spitzer KW & Vaughan-Jones RD (2005). Experimental generation and computational modeling of intracellular pH gradients in cardiac myocytes. *Biophys J* **88**, 3018–3037.
- Swietach P & Vaughan-Jones RD (2005). Relationship between intracellular pH and proton mobility in rat and guinea-pig ventricular myocytes. *J Physiol* **566**, 793–806.
- Swietach P, Tiffert T, Mauritz JM, Seear R, Esposito A, Kaminski CF, Lew VL & Vaughan-Jones RD (2010). Hydrogen ion dynamics in human red blood cells. *J Physiol* **588**, 4995–5014.
- Tappan DV (1968). Carbonic anhydrase activity of erythrocyte ghosts. *Experientia* **24**, 127.

- Vaughan-Jones RD, Peercy BE, Keener JP & Spitzer KW (2002). Intrinsic H^+ ion mobility in the rabbit ventricular myocyte. *J Physiol* **541**, 139–158.
- Vince JW, Carlsson U & Reithmeier RA (2000). Localization of the Cl^-/HCO_3^- anion exchanger binding site to the amino-terminal region of carbonic anhydrase II. *Biochemistry* **39**, 13344–13349.
- Vince JW & Reithmeier RA (1998). Carbonic anhydrase II binds to the carboxyl terminus of human band 3, the erythrocyte Cl^-/HCO_3^- exchanger. *J Biol Chem* **273**, 28430–28437.
- Vince JW & Reithmeier RA (2000). Identification of the carbonic anhydrase II binding site in the Cl^-/HCO_3^- anion exchanger AE1. *Biochemistry* **39**, 5527–5533.
- Yamada H, Horita S, Suzuki M, Fujita T & Seki G (2011). Functional role of a putative carbonic anhydrase II-binding domain in the electrogenic $Na^+ -HCO_3^-$ cotransporter NBCe1 expressed in *Xenopus* oocytes. *Channels (Austin)* **5**, 106–109.
- Zaniboni M, Swietach P, Rossini A, Yamamoto T, Spitzer KW & Vaughan-Jones RD (2003). Intracellular proton mobility and buffering power in cardiac ventricular myocytes from rat, rabbit, and guinea pig. *Am J Physiol Heart Circ Physiol* **285**, H1236–H1246.

Additional information

Competing interests

None.

Author contributions

S.A-S., V.E., S.P., R.J.S. and J.D.M. performed the experiments; W.S.S. and J.P.C. provided samples of CAII-deficient blood, and S.L.A. provided plasmids; V.E., S.A-S., S.P. and G.G. designed the research and wrote the paper; W.S.S., J.P.C. and S.L.A. suggested additional experiments and revised the manuscript.

Funding

This work was supported by DFG grant EN 908/1-1.

Acknowledgments

We thank Dr V. Bennett for providing hANK1 cDNA, Robert Freund for cloning of pcDNA3-3xFlag-hAE1 and Dorothee Krone for technical assistance.